

Bio-inspired Robotics based on Liquid Crystalline Elastomers(LCEs) and
Flexible Stimulators

by

Qingyang Sun

B.S., Huazhong University of Science and Technology, 2016

A thesis submitted to the
Faculty of the Graduate School of the
University of Colorado in partial fulfillment
of the requirement for the degree of
Master of Science
Department of Mechanical Engineering

2018

This thesis entitled:
*Bio-inspired Robotics based on Liquid Crystalline Elastomers(LCEs) and
Flexible Stimulators*
written by Qingyang Sun
has been approved for the Department of Mechanical Engineering

Prof.Jianliang Xiao

Prof. Yifu Ding

Date_____

The final copy of this thesis has been examined by the signatories, and we
find that both the content and the form meet acceptable presentation
standards
of scholarly work in the above mentioned discipline.

Qingyang Sun (M.S. Mechanical Engineering)

Bio-inspired Robotics based on Liquid Crystalline Elastomers(LCEs) and Flexible Stimulators

Thesis is directed by Professor Jianliang Xiao

Abstract

Soft robotics are most inspired from animals harnessing soft structures to move on ground or even harsh topological surface. Soft materials are the primary composition of soft robotics. Although they are not as durable and strong as ceramics and metals, soft materials stand out for their reversibility of deformation, response to stimuli and bio-compatibility. In this dissertation, liquid crystalline elastomer(LCE) combined with patterned flexible electronics and liquid metal have been used as soft robotics that simulating different kinds of worm-like movement. Besides, the impressive bendability of LCE finds itself a lot of potential in nature-camouflage area.

First of all, the conception of soft robotics was deeply dug out through references about smart materials, for example, shape memory alloy(SMA), shape memory polymer(SMP), liquid crystalline elastomer(LCE) and etc. In this dissertation, LCE, as an advanced smart material, is used to fabricate soft robots, simulating inchworm movement. Another key point is the designation of actuator, in the research, flexible electronics were integrated onto LCE strip, when voltage was applied, the electronics increased temperature of specific part on one side of strip. Temperature difference

between top and bottom surface induced LCE bending to approach anticipated location. Several cycles of inchworm movement were achieved, change in actuation sequence induces an inverse movement direction. Secondly, an improvement was carried out for crawling robots with combination of liquid metal(LM). Different from flexible electronics which are actually solid, “liquid electronics” suits more in the term “flexible”. Liquid metal was introduced into the research due to elevated requirement of bending curvature for its freely and reversibly transition between solid and liquid. New attachment approach was carried out using passive PDMS layer embedding to solidify contact between liquid metal and LCE. As consequence, the soft robotics could grasp a stick and move itself towards bi-direction. Repeatability test was conducted for the composite bending, twisting and shrinking.

Last but not the least, the LCE/LM system patterned in different shape could easily camouflage itself as black agaric, seaweed and origami pentagram, in another word, the potential application in camouflage of this structure was developed. In specific parts of passive eco-flex layer, LCE segments were embedded and connected by liquid metal channels. For example, to simulate black agaric, four or five spots of the system were expected to bend, when external input was applied, LM in these areas generate and conduct heat around causing bending and maintaining the system at a specific shape, also,

black paints were cast onto composite in advance. Repeatability test was conducted and reported.

*This dissertation is dedicated to my grandfather
Zhenyi Sun, my parents Shaoren Sun, Fengxian
Zheng, and my brother Qingbin Sun.*

Acknowledgement

My dissertation would not be accomplished without help from many people during my master period. I'd like to take this opportunity to express my cordial gratitude to thank to all who has contributed to my academic endeavor during my two years of master study.

First, I would like to express my deepest gratitude to my supervisor, Prof. Jianliang Xiao for his all-time supporting and guidance. The moments will be imprinted in my heart that he taught me how to improve presentation skills, how to organize a paper, and how to forecast then solve potential research problems, which is so encouraged to contribute for my future endeavor.

Besides, I'd also want to thank Prof. Xiao for his powerful recommendation in my PhD's application.

Secondly, I also want to thank Prof. Yifu Ding and Prof. Mark Rentschler for treasured time to attend my thesis defense as committee. I gratefully appreciate their suggestions and comments to improve my speech skills. I also want to thank to Prof. Y.C. Lee, and Prof. Franck Vernerey for their strong recommendations in my PhD's application.

In addition, I would like to thank to my collaborators: First, special thanks to Zhanan Zou in my group. He is not only my collaborator but also a guider as well. Thanks for his all-time advice and comments on my research, I'll remember the days we spent working and discussing in the lab seeking for

better solutions. Besides, thanks to Dana Francesca Stamo for her supports during complicated experimental processes, and Hanzon Drew from Prof. Kai Yu's group at CU Denver for their robust materials.

Also, I would like to thank to my lab-mates Yu Wang, Andres Villada, Yinding Chi, Yan Li, Chuanqian Shi, and Sichong Li for their help and sparkled ideas during my research studies. It's my great honor to work with so many friendly colleges and intriguing minds.

Finally, I would express my love to my family. My parents, thanks them for their raising up and life-time education. I'm grateful for their scarification and supporting. I hope I haven't let them down.

Contents

Chapter 1 Introduction.....	1
1.1 Soft Robotics Review.....	1
1.2 Soft Robotics Simulation.....	6
1.2.1 Inchworm Locomotion.....	6
1.2.2 Camouflage System.....	7
1.3 Liquid Metal as Stimulator in Soft Robotics.....	10
Chapter 2 Inchworm Locomotion Simulation achieved by Liquid Crystalline Elastomers (LCEs) and Flexible Electronics (FEs).....	14
2.1 Introduction.....	14
2.2 Experimental Section.....	15
2.2.1 Preparation of Inchworm Robot.....	15
2.2.2 Robot Movement Simulation.....	17
2.3 Results and Discussion.....	19
2.4 Conclusion.....	24
Chapter 3 Improved Soft Robotics Combining with Liquid Metal (LM)	26
3.1 Introduction.....	26
3.2 Preparation of LCE/LM System.....	26
3.3 LCE/LM System Deformation Performance.....	28
3.4 Fabrication of Enhanced Robot.....	31
3.5 Conclusion.....	34
Chapter 4 Reversibly Deformable Robotics blend into Surroundings.....	35
4.1 Introduction.....	35
4.2 Experimental Section.....	36
4.2.1 Preparation of Camouflage Robot.....	36
4.2.2 Camouflage Phenomena Simulation.....	37
4.3 Conclusion.....	41
Chapter 5 Summary and Prospects.....	43
5.1 Summary.....	43
5.2 Prospects.....	44
Bibliography.....	46

Tables

Table

1-1 Properties of Gallium, Mercury and Rubidium.....	11
2-1 Comparison of two inchworm systems.....	25

Figures

Figure

1-1 dielectric elastomer soft robotics.....	2
1-2 mechanism of LCE actuation.....	4
1-3 two applications of LCE.....	5
1-4 inchworm simulation.....	7
1-5 camouflage system in nature and human society.....	8
1-6 progression in camouflage research field.....	9
1-7 Applications of liquid metal.....	12
2-1 demonstration of sandpaper-inchworm system.....	17
2-2 demonstration of 3d-printed-legged robot.....	18
2-3 dynamic bending performance for LCE strips.....	21
2-4 ultimate state of LCE samples in respond time and bending angle.....	22
2-5 dynamic displacement of two inchworm systems.....	23
3-1 configuration of LCE/LM system and the performance	29
3-2 dynamic deformation performance and repeatability test.....	30
3-3 PDMS-casting samples and designed robots.....	32
3-4 bending performance of PDMS-casting sample.....	33
4-1 Designation, fabrication, actuation and FEA analysis for three camouflage systems.....	38
4-2 deformation of camouflage robots with painting.....	39
4-3 Illustration of moving-camouflaging robot.....	41

Chapter 1 Introduction

1.1 Soft robotics Review

When it comes to robotics, the very first thought hit into minds is the rigid, cold and kind of merciless humanoid machine. In recent decades, silicon stands out in electronic field for its semi-conducting property, which could freely send and receive “on” and “off” signals, the respond to input stimuli contributes to conception of robots. However, soft materials share the same mechanism that respond to other stimuli such as voltage [1-3], temperature [4-6], magnetic field [7-9] and frequency range of light [10-12]. These characteristics make them deform to a desired shape, therefore, controlled locomotion, deformation and specific functions are achieved. Those materials are called smart materials.

Varieties of smart materials have been discovered [13-25]. For example, shape memory alloy(SMA) [13,14], shape memory polymer(SMP) [15] and liquid crystalline elastomer(LCE) [10-11,16-20]. Those materials react due to its own properties in a molecular level. Another example such as pneumatic [21,22], dielectric [1-2,23-24] and hydraulic [23,25] materials are just harnessing its inner actuation and easy-deformable characteristics. Dielectric

materials have similar mechanical properties as human skin, and could be actuated by electrical voltage. Figure 1-1(a) shows a dielectric elastomer

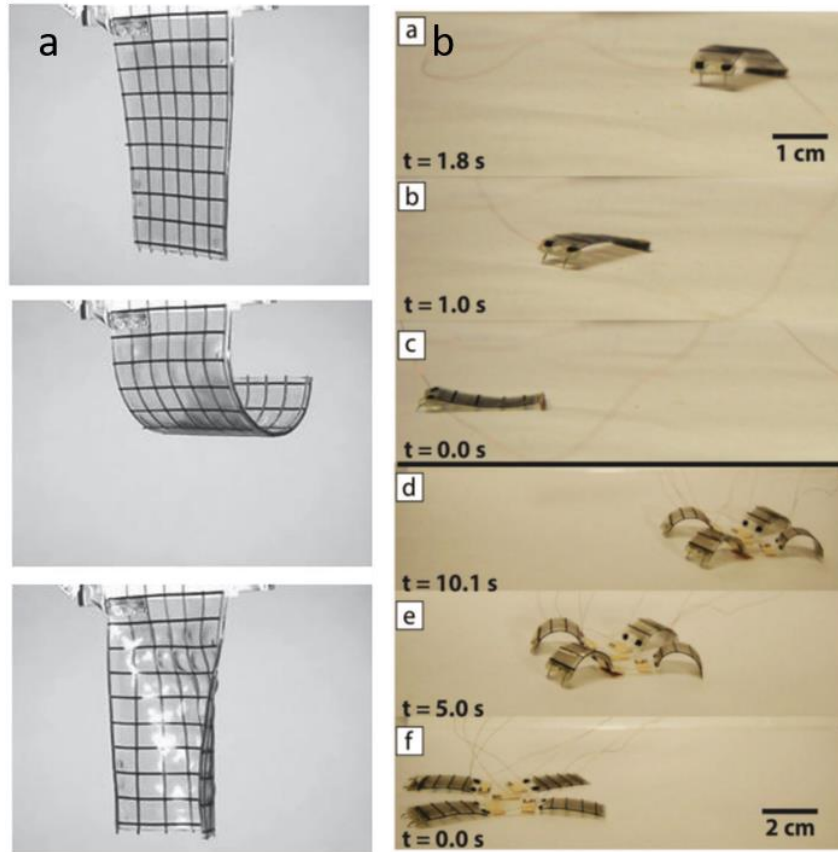


Figure 1-1. [2] a) Bilayer of two dielectric elastomer actuators bonded together with fibers oriented at 0° and 90° in each layer. When horizontally fiber is actuated, bending curvature is vertical (second picture) whereas in third picture when vertically fiber is actuated the bending curvature is horizontal. [24] b) Demonstrations of walking ability and speed. An active layer inchworm actuator actuated at 10Hz (a-c). A four-legged crawling robot actuated at 1.5Hz (d-f).

gripper bending horizontally and vertically [2], the sheet of elastomer becomes thinner in response to Maxwell stress between charges when voltage is applied. The Maxwell stress is given by $\sigma_z = -\epsilon E^2$ where E is electrical field and ϵ is permittivity of elastomer layer. A bilayer of two dielectric actuators bonded together with fibers aligned horizontally and vertically.

When side with horizontally fiber is actuated, bending curvature is vertical whereas when side with vertically aligned fiber is actuated, the bending curvature is horizontal. Cylindrical actuator consisting of an elastomer sleeve attached to a series of stiff rings and stiff strip or fiber are attached to the elastomer are controlling bending directions. Another dielectric elastomer application [24] shows in Figure 1-1(b), a crawling or walking robots with bended needles as feet are achieving movement. Four-legged robots and simpler inchworms are fabricated, crawling speed is directly proportional to driving frequency of voltage “on” and “off”, as frequency increased, slipping occurs and speed reaches a plateau while at high frequency the robot could not deform quickly for its movement. Apart from inner actuation materials harnessing electrical, hydraulic and pneumatic triggers, this dissertation focuses more on molecular-deformable materials, especially LCE. LCE consists of properties of elastomers and liquid crystals, they support the materials with rubber elasticity and ability of self-organization. Such properties allow them able to deform reversibly when external stimuli are applied and removed. The preparation of LCE will be discussed later. As shown in Figure 1-2, while at room temperature, liquid crystal polymer chains are anisotropic, when heated above transition temperature, it turns to the isotropic phase, consequently, the sample as a whole will change its shape [26]. Therefore, the deformation could be achieved by both temperature

variation and isothermal shift of phase transition temperatures.

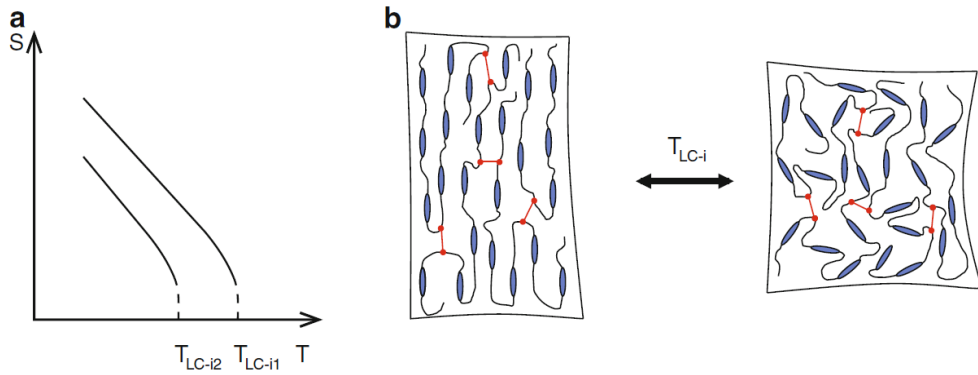


Figure 1-2. [26] (a) Anisotropy of LC phase as expressed in order parameter S , leads to an anisotropic conformation of polymer backbone. The magnitude of chain anisotropy is generally assumed to have the same temperature dependence. It decreases with increasing temperature and jumps to zero at clearing temperature (T_{LC-i1}). By photoisomerization of dyes it is possible to shift temperature (T_{LC-i2}). (b) Change of the order at clearing temperature. At isotropic phase the polymer chains adopt a random coil conformation, leading to a macroscopic deformation of the sample.

Couples of LCE applications are covered [10-11,16-20], Hao Z. [10] fabricated light-fueled microscopic walkers. The light sensitive element (azo-dye) is designed to be activated by green light (495-570nm in wavelength). In the experiment, the walker is actuated by chopped 532nm laser excitation, the composition and movement are shown in Figure 1-3 (a), the mechanical response to light is fully reversible and consists in a contraction of around 20% along director. The response time is also recorded around 10ms at 100Hz of laser excitation. Another intriguing application is in energy harvesting field, Chensha Li [11] made an artificial heliotropic devices that could follow the sun for increased light interception. The device is using reversible photo-

thermomechanical LCE nanocomposite that directly actuated by the natural sunlight. Consequently, solar cells in the devices produce significant photocurrent output comparing to normal solar cells. The schematic is shown in Figure 1-3 (b), solar cells are installed on a platform connected with actuators and elastically supported. At any time, actuators facing incoming sunlight would be in contracted state while others in relax state. As a result, the platform driven by contracted sunlight would incline itself to incoming sunlight direction, hence the increased shined area and photocurrent output.

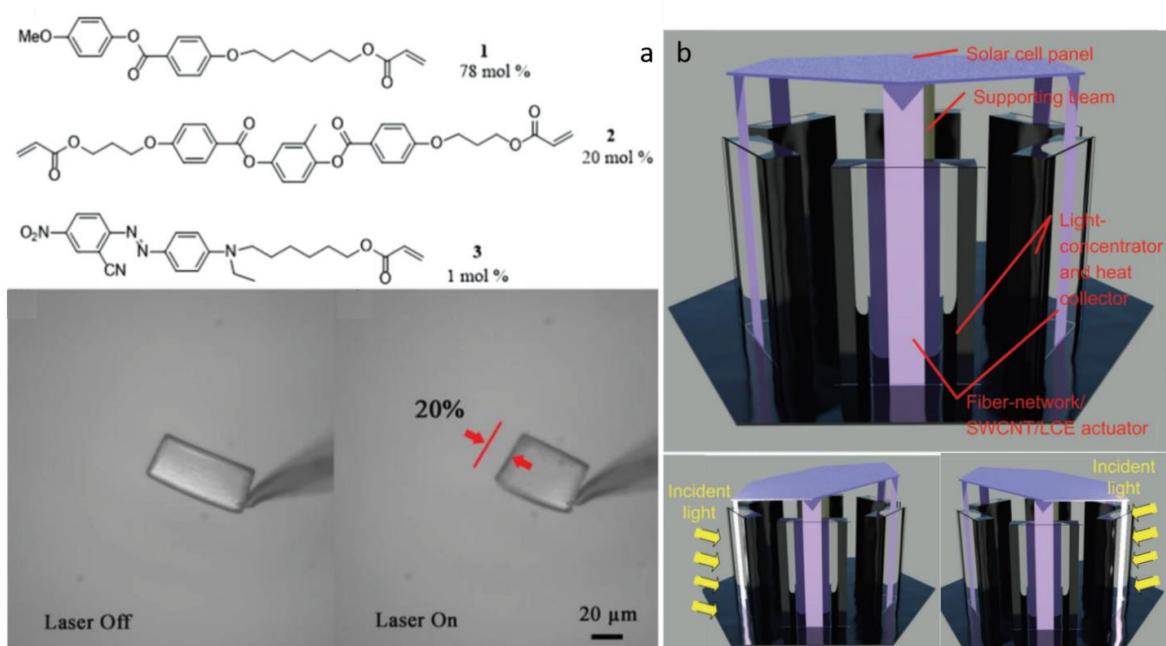


Figure 1-3. [10] (a) LCE monomer composition used in experiment (up) and 60*30*10 μm³ LCE actuator contracted 20% along the long axis while heated above 100°C by laser beam (down). [11] (b) Schematic of artificial heliotropism (up) and its response to incident natural light (down).

1.2 Soft Robotics Simulation

Most of soft robotics ideas were borrowed from nature, animals and plants take advantage of soft structures to do complicated movement. The most typical one is muscular structure in animals (e.g. elephant trunk and starfish feet) that composed of soft muscle tissues and could exhibit movement easily. Apart from simulation of soft robotics shape and function, another considerable issue is the control system that allow robots interact with environment. Two simulations are mainly discussed.

1.2.1 Inchworm Locomotion

Simulation of inchworm locomotion has been conducted through recent decades [27-30]. The inchworm consists of front end, rear end and middle part. Each part or end are composed of several segments to cause bend. Several legs are under ends part as anchors. When movement starts, front legs anchor onto ground surface followed by middle part buckling up, then anchors the rear legs while release front anchor and relieve middle part buckle stress. The steps are shown in Figure 1-4 (a). H.Guo [29] designed pneumatic actuated inchworm with silicon tube and chamber. To prevent soft actuators inflating into various directions that deform like a balloon, the pneumatic actuator was laid with the strain limiting layers, hence, the silicon tube can exhibit desired deformation. In the meantime, actuator was

wrapped with inextensible fibers in case of expanding radially. Equipped with legs, the robot shows great performance in simulating inchworm as shown in Figure 1-4 (b). The air cavity in the body section was designed to exhibit the omega deformation, anchor-motion mechanism was achieved by feet in front and back sections. The figure also shows the robot in original state (Fig1-4 (b)-(1)), actuated state (Fig1-4 (b)-(2), (3)), and reset to original state (Fig1-4 (b)-(4)). The response time of inflating and deflating for the soft robot were 0.5 seconds and 1.5 seconds, at this period, the robot shows the average velocity of 240cm/min. Even the feet may slide backward during motion process, total efficiency won't be affected.

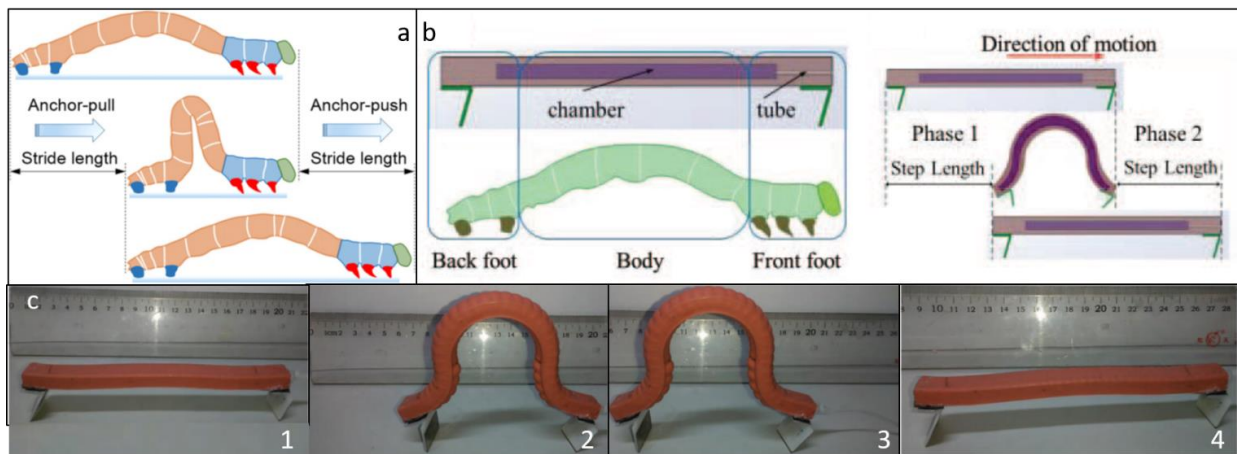


Figure 1-4. [27] (a) Locomotion of an inchworm for one stride [29] (b) Structure comparison between the robot structure and an inchworm (left). Locomotive procedure for a period of motion of the robot. [29] (c) Motion sequence for the inchworm-type robot.

1.2.2 Camouflage System

Camouflage has always been one of the most intriguing field in research, animals and even some plants blend themselves into surroundings so that

predators could be deceived by undistinguishable features or be warned of weird or dizzy costumes. Basically, camouflage could be sorted as change in colors, shapes, patterns, and others (odor, noise, motions), etc. The most straightforward example is chameleon, which is known for its color changing to vanish itself into environment. Apart from chameleon, amounts of animals have obtained protective coloration through generations of evolution. Figure 1-5 shows (a) orchid mantis, (b) mossy frog, (c) rattlesnake and (d) chameleon blends into the surroundings by their disguise through shapes, colors, and patterns.

Besides, in the human society, this trick is widely employed in military for hiding soldiers from enemies' sights. Figure 1-5 (e) shows a soldier is disguising himself with bush-like paints.



Figure 1-5. (a) Orchid mantis shares the similar structure with orchid petals; (b) Vietnamese Mossy Frog blends into moss-covered ground; (c) Rattlesnake shows similar color with ground; (d) Chameleon could sense surrounding colors and suit itself with it; (e) Soldier disguising himself with green camouflage. *pinterest.com, google.com*

Apart from employment in nature and military, the use of camouflage has also been developed in soft robotics field. With the functional enhancement in soft robotics, scientists started to take advantage of natural tricks into soft systems [31], including dynamic change in coloration, luminescence, pattern and shape, potentially improved its adaptability in nature or some harsh environments. Nature offers many approaches to get structural colorations, based on which, scientists are inspired to employ biomimetic photonic materials with tunable coloration [32]. Figure 1-6 shows examples of accomplished soft robotics that can camouflage or tune colorations [31, 33-35]. Figure 1-6 (a) shows a pneumatic-controlling robot fabricated by Stephen's group [31] walking to rock bed and red leaves, then conceal itself into surroundings by embedded pigment channels. Different patterns of

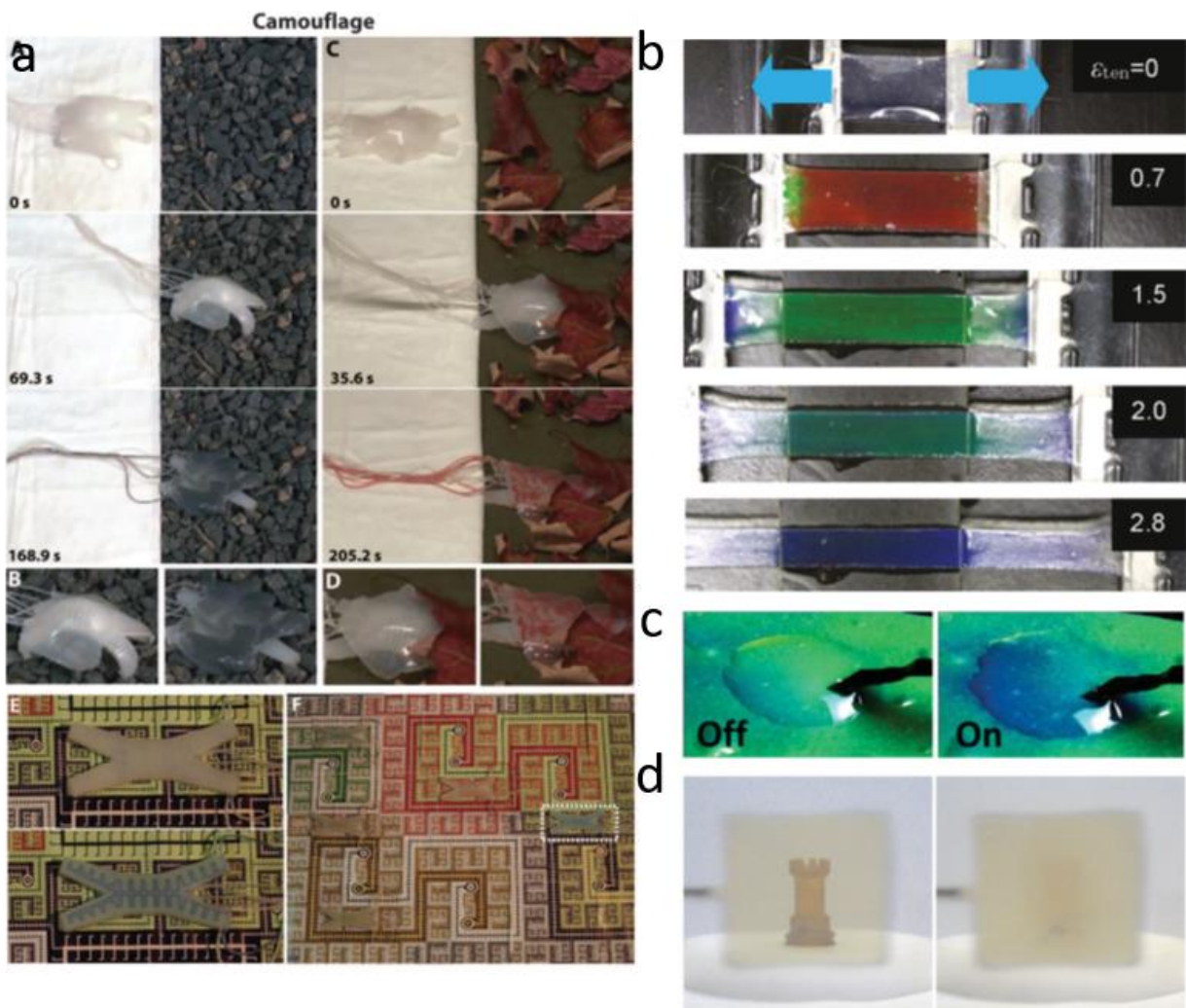


Figure 1-6. (a) Robot walking on a rock bed and red leaves then camouflaged by

pumping pigment dispersions through microfluidic channels (top), Uncamouflaged and camouflaged robot in a man-made environment; (b) Tunable colors in hydrogel with microdomains of bilayers periodically stacked in polymer; (c) Tunable structural color by DE actuators and polymer opals; (d) Electrically triggered surface wrinkling of elastomeric coatings changes appearance of coating from transparent to translucent.

channels could be designed to suit the robot for different environments.

Figure 1-6 (b) shows a rubberlike elastomeric hydrogel with microdomains of bilayers periodically stacked in polymer networks [33]. The hydrogel is able to change color over the entire visible spectrum. Figure 1-6 (c) shows an example of voltage-tunable structural colors change that achieved by combination of polymer opals and dielectric elastomers [34], the color is controlled by voltage. Figure 1-6 (d) depicts surface wrinkling phenomenon of elastomeric coatings [35]. In the flat state (left), the polymer is transparent, while by applying voltage across elastomeric coatings, the elastomer becomes translucent in a wrinkled state (right).

1.3 Liquid Metal as Stimulator in Soft Robotics

In the research, liquid metal is introduced into the soft systems for its flexibility, robustness and great thermal conductivity. Liquid metal is such kind of alloy with low melting temperature and in liquid phase around room temperature. Compared to non-metallic liquids, liquid metal has a higher thermal conductivity and electrical resistivity, while compared to solid

metals, liquid metal shows its great flexibility, robustness and more freely reversible transformation from solid state to liquid state. Besides, liquid metal is also an economical metal that could be totally affordable in research.

Name	Gallium	Mercury	Rubidium
Atomic number	31	80	37
Atomic Weight	69.723	200.59	85.468
Melting Point(°C)	29.76	-38.83	38.89
Thermal Conduct	40.6 W/(m ·K)	8.3 W/(m ·K)	58.2 W/(m ·K)
Electrical Resistivity	270 nΩ ·m (at 20 °C)	961 nΩ ·m (at 25 °C)	128 nΩ ·m (at 20 °C)
Price(\$/kg)	~400	~900	~6000

Table 1-1. Properties of Gallium, Mercury and Rubidium

Here we list three most commonly used liquid metals which are Gallium, Mercury and Rubidium as shown in Table 1-1. The melting point of three metals vary from -38.83°C to 38.89°C, thermal conductivity and electrical conductivity are significantly higher than non-metallic liquids. Gallium and

Mercury are the cheapest materials. Also, with consideration of toxicity, Mercury will not be the option for mercury vapor is toxic. To conclude, according to their properties, price and toxicity, Gallium is the optimal choice to use as a flexible stimulator. The gallium has a relative high thermal conductivity about $40.6 \text{ W}/(\text{m}\cdot\text{K})$, low electrical resistivity of $270 \text{ n}\Omega\cdot\text{m}$ at 20°C and about 400 dollars per kg for price.

Liquid metal shows great flexibility that could withstand mechanic bending and stretching under use of voltage [36], applications of liquid metal has been developed in artificial skin [37,38], stretchable conductors [39-42], inherently aligned microfluidic electrodes [43], compliant MEMS components [44,45], microfluidic heat sinks [46] and antennas [47-55], as shown in Figure 1-7.

Figure 1-7 (a) shows an ultra-stretchable wire made by injecting liquid metal

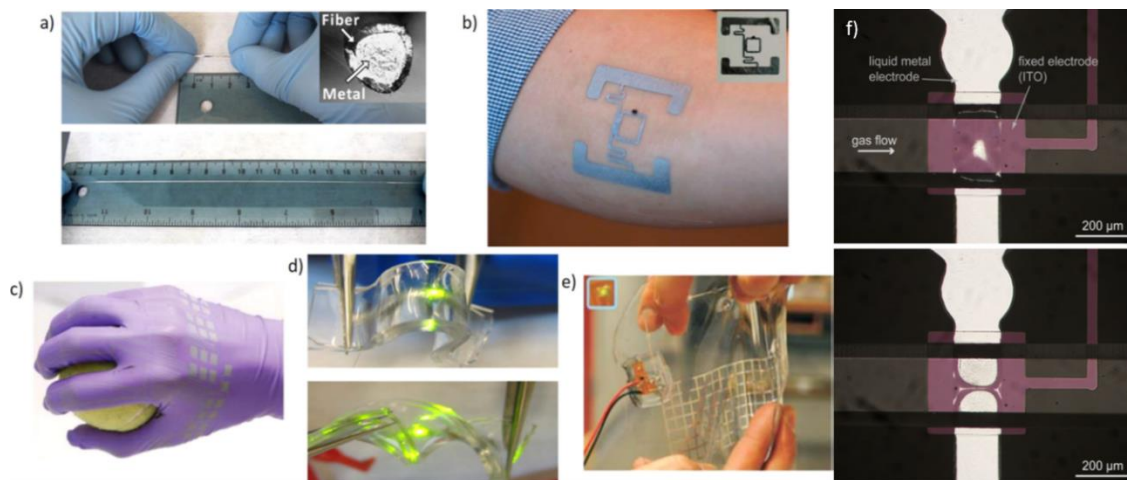


Figure 1-7. [41] a) Ultra-stretchable wire with LM inside hollow elastomeric fiber. [56] b) LM stretchable RF identity tag. [42] c) Nitrile glove functionalized by inkjet-printed LM particles. [39] d) LED integrated into polymer with LM interconnects. [50] e) LM RF strain sensor. [44] f) On-chip microvalve used in gas channel.

into a hollow elastomeric fiber is stretched to 10 times of its original length. Figure 1-7 (b) demonstrates a stretchable/conformable RF identity tag that could attach to human skin. Figure 1-7 (c) illustrates liquid metal inkjet-printed onto a nitrile glove holding a tennis ball showing the stretchability of electronics. Figure 1-7 (d) shows an example that liquid metal combined with LED could be integrated into polymer and undergo bending and twisting. Figure 1-7 (e) depicts a bi-axial RF strain sensor. Besides from its potential in stretchable circuitry, liquid metal could also be employed in other fields. Figure 1-7 (f) delivers the idea of on-chip microvalve composed of fixed electrode and liquid metal electrode, when voltage potential is applied, liquid metal is driven by electrostatic pressure to collapse PDMS and close the valve (bottom).

Chapter 2 Inchworm Locomotion Simulation achieved by Liquid Crystalline Elastomers (LCEs) and Flexible Electronics (FEs)

2.1 Introduction

Soft robots have been developed significantly over recent decades, soft materials that could respond to external stimuli become more compliant than traditional cold, metal-clad, and humanoid machines. Especially with inspiration granted by nature, scientists fabricated numerous bio-inspired robots that employed in specific jobs. A few researches have been conducted to simulate inchworm for its special movement methods. Koh et al [57] fabricated such inchworm called Omegabot made of SMA springs and smart composite microstructures. Lee et al [58] designed a motor-actuated inchworm robot with bidirectional claws. Ueno et al [59] used electroconjugate fluid to produce body deformation and suction achieving two-way movement. Wang et al [27] made bilayer bending moving robot composed of SMA and Silicone.

In this study, a new designation of inchworm movement simulation has been brought out by composing LCE strip and patterned flexible electronics (FEs). The LCE strip was used to actuate the bending, FEs taped on top or bottom surface of LCE were connected to outer battery and generated heat to

stimulate specific bending part of actuator, when the FEs stimulated, temperature difference between top and bottom surface led to two different magnitude of shrinking which induced the bending. Different LCE samples were programmed in different thickness, the optimal thickness to reach maximum bending magnitude and shortest respond time were demonstrated. The bending performance varies from sample thickness and external current. For 1.1mm thickness sample under 2A input, a relative small bending angle was observed and took about 80 seconds to reach such a bending amplitude. When current input increased, the bending angle went up steadily with respond time decreasing significantly. For 1.3mm thickness sample, it took longer time when 2.25A was applied since more time was needed to reach a relative larger bending angle. Same phenomenon was observed for 1.8mm thickness sample.

2.2 Experimental Section

2.2.1 Preparation of Inchworm Robot

The inchworm sample composed of LCE strip and patterned flexible electronics, the LCE was prepared using a two-stage thiol-acrylate Michael addition-photopolymerization (TAMAP) reaction. 4-bis-[4-(3-acryloyloxypropyloxy) benzoyloxy]-2-methylbenzene (RM257), pentaerythritol tetrakis(3-mercaptopropionate) (PETMP), 2,2-(ethylenedioxy) diethanethiol (EDDET), (2-hydroxyethoxy)-2-methylpropiophenone (HHMP)

and dipropylamine (DPA) which were used as received purchasing from Sigma Aldrich except RM257 bought from Wilshire Technologies. 4g of RM257, 0.217g of PETMP, 0.9157g of EDDET and 0.0257g of HHMP were dissolved into 1.6g of toluene solution. 0.568g of DPA (diluted with toluene at a ratio of 1:50) was added into solution for the first polymerization then cured at 80°C for 12h. The cured polymer was then aligned by stretching and exposed to UV light for at least 15mins as the second polymerization.

The flexible electronics used as heaters were made from aluminum foil with thickness of 100µm from Reynolds Wrap. The original aluminum foil protected by water-soluble tape (Aquasol Corporation) was first cut by mechanical cutter (Silhouette CAMEO) with designed patterns, and then transformed onto LCE samples with black tape (Nisshin EM. CO., LTD), three specific parts of LCE sample were taped with the heaters aforementioned. The heaters were connected to an outer battery that supply current to generate heat stimulating specific bending part. What's more, two sandpaper pieces were taped beneath head and tail part of LCE strip, they were used as friction-increasing feet to anchor onto ground surface. The process is demonstrated in Figure 2-1 (A).

For another sample of inchworm system, we designed and integrated two 3-d printed legs onto both head and tail part of LCE strip, and only one heater

taped beneath middle part. The feet were designed to move the robot in only one direction.

2.2.2 Robot Movement Simulation

To simulate inchworm locomotion, the process of its movement was first studied, the movement is achieved by synergetic work done by its front legs, rear legs and middle actuating part. When it moves, the rear legs are the

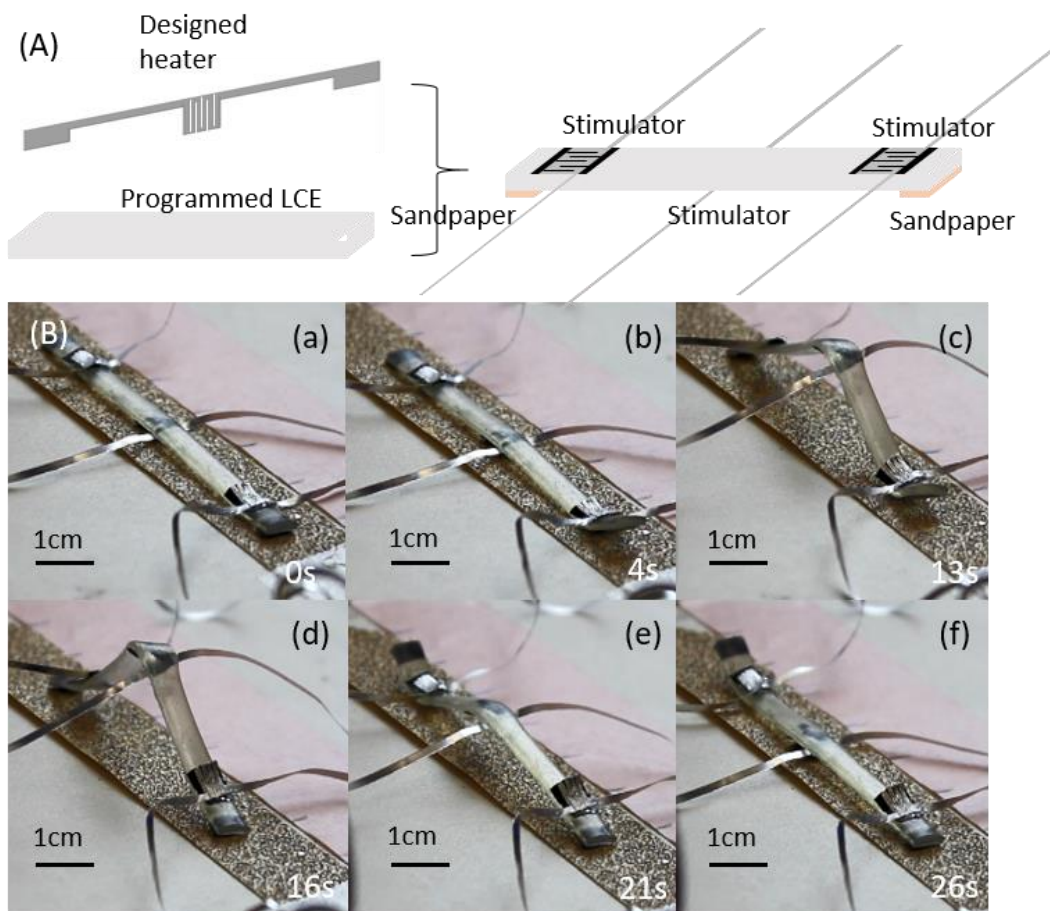


Figure 2-1. A) Demonstration of sandpaper-inchworm system, three designed heaters connected with outer battery were taped onto LCE strip surface, two sandpaper pieces were taped under head and bottom part as friction-increasing feet. B) Illustration of inchworm system movement. At 0 seconds, the robot was at rest state (Fig2-1(B)-(a)), then with stimulation of tail heater, tail part bended up ((B)-(b)) with less friction of rear feet. Middle heater was next to stimulate, causing body

part arching ((B)-(c)), with relaxing of body part, rear foot attached to sandpaper again to obtain friction ((B)-(d)) while front foot detaching from ground ((B)-(e)). At last, the arching was eliminated with each end reset to original shape, while a little strain residue was observed for front end ((B)-(f)).

first to move towards head part until most of the body show arching, during which process, the front legs remain stationary. Then the rear legs become anchored followed by middle body part relaxing while front legs detach from ground. After all the parts reset to original shape, one step is completed.

For our first inchworm system which equipped with sandpaper feet, the

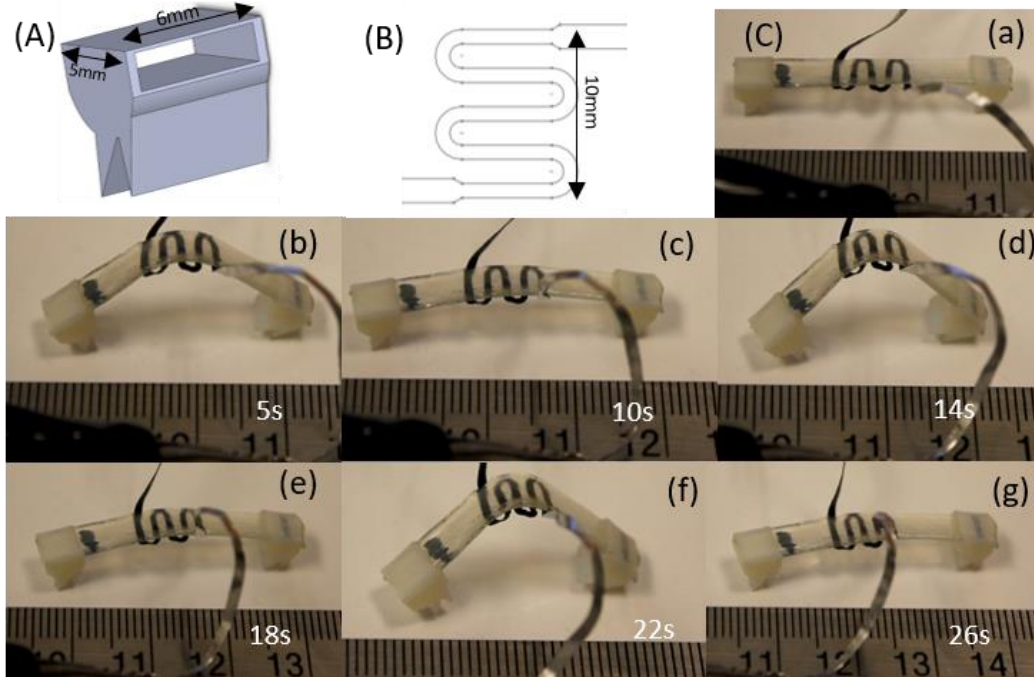


Figure 2-2. A) 3D-printed leg with two feet in a specific angle that move the robot in only one way. B) Designed serpentine structure heater connected to an outer battery. C) three cycles of inchworm system movement were depicted. At 0s ((C)-(a)), the robot was at rest state, (b)-(c) shows the first cycle of stimulation and relaxation which took about 10 seconds, while the second and third cycle took about 8 seconds. After three cycles, three centimeters of displacement was achieved.

whole system was placed onto a sandpaper, so in one stride of locomotion, tail heater was the first to stimulate, causing tail part bends up and less friction on rear foot, and followed by middle heater stimulating to arch the whole body, the tail heater was disconnected, the rear foot attached to the sandpaper again while head part detached causing low friction of front foot, after relaxing of body part and re-attaching of front foot, one stride was completed, as shown in Figure 2-1 (B).

Apart from the sandpaper feet robot, another 3-d printed legs-equipped robot was designed and fabricated as shown in Figure 2-2. The feet (Figure 2-2 (A)) were designed specifically that it could move the robot in only one way by alternatively self-anchoring and detaching. Besides, only one heater (Figure 2-2(B)) is enough for the stimulation. Several cycles were achieved by this system as shown in Figure 2-2 (C).

2.3 Results and Discussion

For programmed LCE samples, the bending performance was test for different thickness under varied current input. The samples were fabricated in 1.1mm, 1.3mm and 1.8mm thickness, current input varies from 2A to 2.75A. For testing, a heater was attached on middle part while one half of sample was fixed with tape horizontally. Therefore, when heater works, the other half of LCE sample bends, and the bending performance in different

conditions were recorded dynamically and statistically. The dynamic deformations of three samples were shown in Figure 2-3, also the performance comparison under 2.75A.

Figure 2-3 (A)-(C) shows 1.1mm, 1.3mm and 1.7mm samples dynamic bending angle under varied current, we could tell that with increasing of current input, the sample shows an enhanced performance for its bending, i.e., the bending angle goes up significantly while the time to reach the max bending angle (respond time) decreases on average. Figure 2-3 (D) integrated three samples performance under 2.75A input, it took longer for 1.8mm sample to reach its max bending amplitude and less time needed for 1.3mm and 1.1mm samples to respond. Besides, Figure 2-3 (E) and (F) quantified the max bending angle and respond time separately, from the figures, we could see that for 1.1mm sample, it took about 15 seconds to reach at 140° of bending angle, 17 seconds to reach at 125° for 1.3mm, 65 seconds to reach 110° for 1.8mm. In another word, a thinner sample shows better bending performance.

The max bending angle and respond time to it were straightforwardly quantified under varied current input for different thickness of LCE samples as shown in Figure 2-4. At 2A input, it took about 80 seconds for 1.1mm

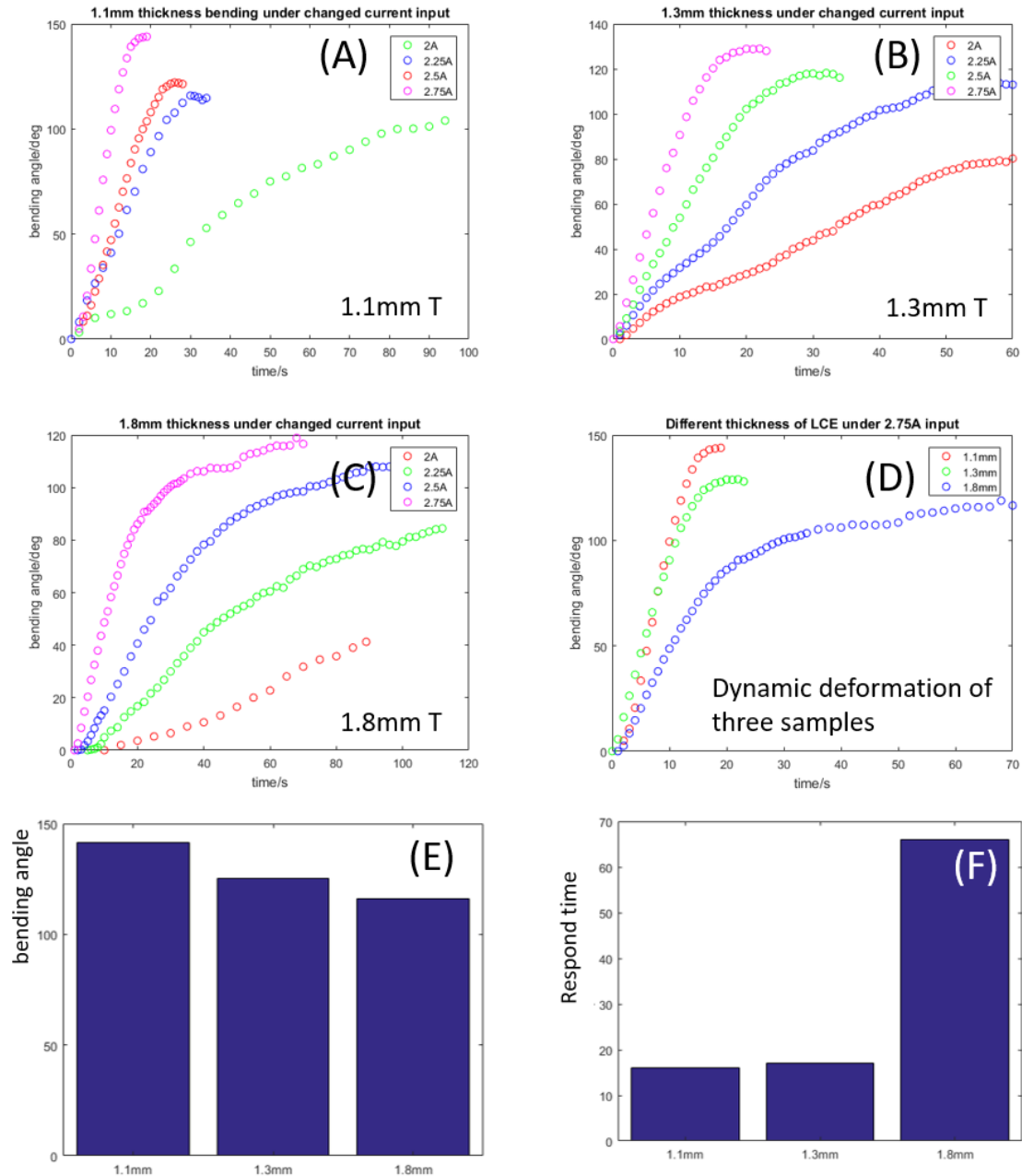


Figure 2-3. Bending performance for each sample (A) 1.1mm sample dynamic bending angle under varied current input, from bottom curve to top: 2A; 2.25A; 2.5A and 2.75A, the same circumstances as (B) and (C). (B) 1.3mm sample. (C) 1.8mm sample. (D) Dynamic deformation of three samples under 2.75 A current input. (E) Max bending angle for each sample, from left to right: 1.1mm, 1.3mm and 1.8mm. (F) Time needed to reach at max bending angle, from left to right: 1.1mm, 1.3mm and 1.8mm.

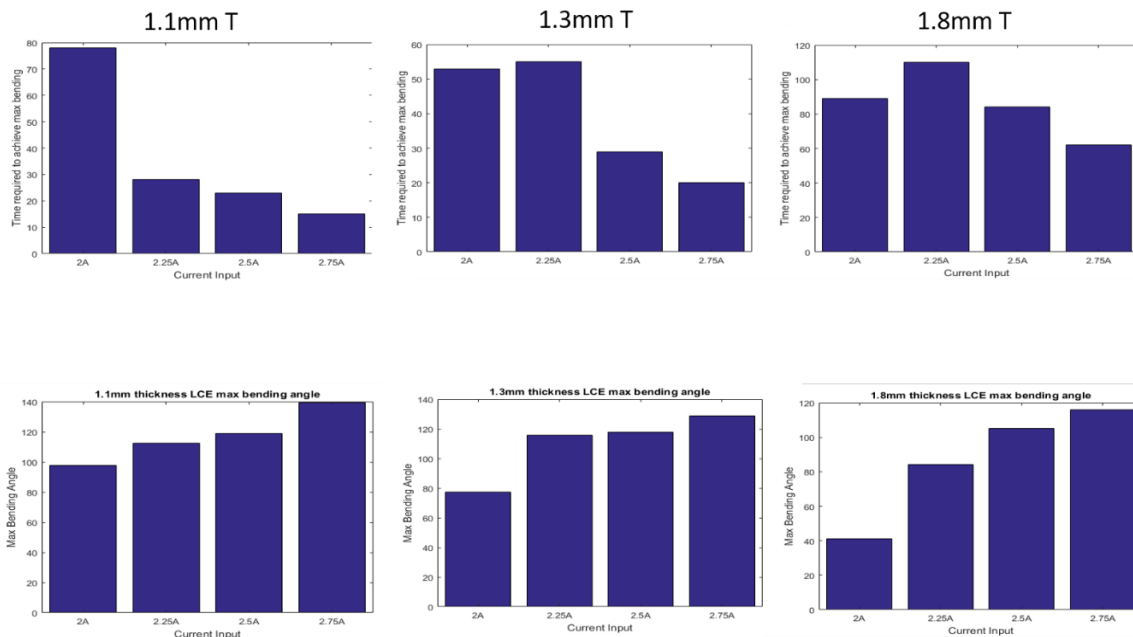


Figure 2-4. Respond time (top) and max bending angle (bottom) for each sample under varied current input, for each figure, the current is 2A, 2.25A, 2.5A and 2.75A from left to right. For example, it takes 80 seconds for 1.1mm thickness LCE sample to reach at 100 bending degree when 2A is applied

thickness to reach 100° of max bending angle, when current input increases, the respond time are shortened magnificently and bending angle increases steadily (left), while for 1.3mm sample, it took a little longer when 2.25A input is applied than 2A input because more time is needed to reach a larger bending angle (middle). While with increasing of input, the respond time

Apart from the basis demonstration of LCE strip bending performance, the movement performance of LCE inchworm systems were also observed (Figure 2-1 (B) and Figure 2-2 (C)) and dynamic movement were recorded as Figure

decreases but still with improved bending angel. The same phenomena are displayed for 1.8mm sample (right).

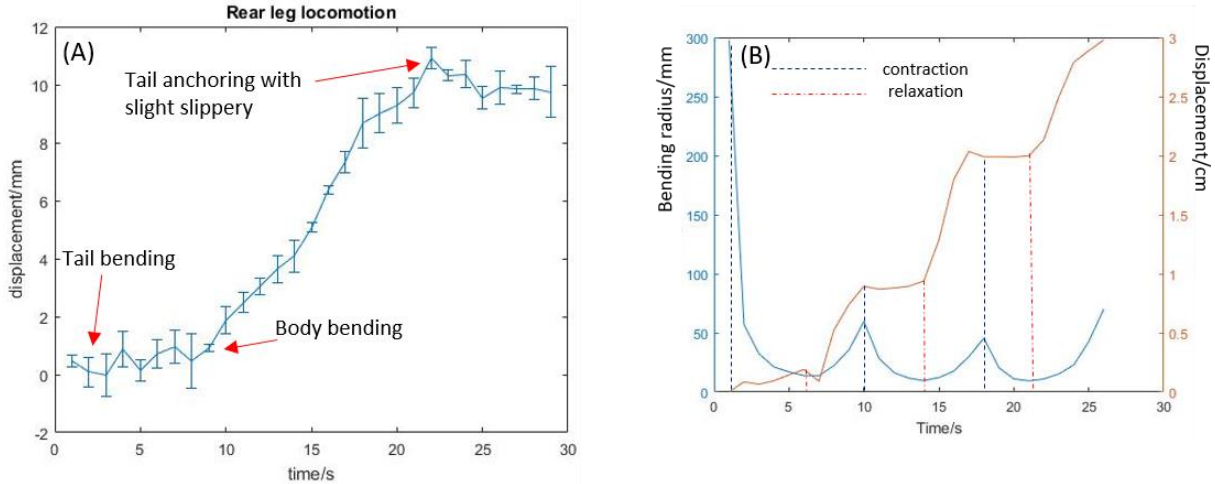


Figure 2-5. Displacement of two inchworm systems (A) Rear leg locomotion of sandpaper robot in one cycle. At the first phase, the tail part bends up without significant movement, then tail part move forwards rapidly with body part shrinking and remains stationary when it attaches to sandpaper again. 1cm of displacement was achieved in one cycle. A slight slippery backwards happens when the body is eliminating arching while it doesn't affect the whole stride. (B) Front foot displacement of 3-d-printed-leg robot in three cycles, brown curve is front foot displacement and blue curve is middle part bending radius. A pre-heat period is observed at the beginning of actuation. During several cycles of contraction and relaxation, 3cm of displacement was made. Slight slippery was also observed that doesn't influence the locomotion.

2-5 showing. Figure 2-5 (A) shows displacement of rear feet of sandpaper robot, Figure 2-5 (B) shows displacement of front leg of 3d-printed leg-robot (brown curve) and middle part bending radius (blue curve). Both figures show a slight slippery when the arching body is eliminating arching, however, the slippery affect so little to the whole stride. Both inchworm system could achieve a displacement of 1cm per cycle.

2.4 Conclusion

In this chapter, a basic demonstration of LCE/FE system has been illustrated, based on its dynamic bending angle, we could see clearly that current input and sample thickness are possible to affect its performance in both max bending amplitude and respond time to reach. As shown in Figure 2-4, we could come to conclusion that the maximum bending curvature is proportional to current input, while responding time relies not only on max bending angle that robot could reach but also the LCE sample thickness. Thickened robot impedes its movement. So, for the samples thickness, the thinner the better, while for current input, the larger the better. However, the exact thickness is designed to satisfy its function, such as holding and carrying stuffs which requires enough thickness to actuate. Also, a larger current input will be preferable than 2.75A to achieve better performance but it takes more time to cool down and hard to remain the robot at a specific shape.

Besides, the comparison of two types of robot has been brought up as shown in Table 2-1.

For the sandpaper feet-equipped robot (left), it is a more complicated system integrated with three heaters, two sandpaper feet, three switches are

controlling in specific sequence. However, the 3d-printed leg-equipped one shows its simplicity in fabrication and actuation process with only one


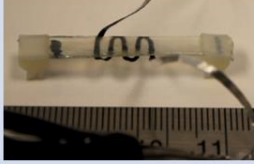
Inchworm Robot	Sandpaper equipped	Printed leg equipped
		
Fabrication Process	three heaters & two sandpaper feet	one heater & two 3d printed legs
Actuation Process	Three switches in specific sequence	One switch
Moving Directions	Forward and backward	One way
Moving Speed	0.5mm/sec	1mm/sec
Special requirement	Sandpaper ground	None

Table 2-1. Comparison between sandpaper feet-system and 3d-printed leg-system

heater, two 3d-printed legs and one switch controlling bending and relaxing. As for the moving characteristics, the former one could achieve two ways moving that towards front and back but at a relative low velocity of 0.5mm/sec, whereas the latter one could only move forward but with a faster speed. At last, the left one needs sandpaper ground to provide its friction while the right one obtains enough friction on the feet to move its body.

Chapter 3 Improved Soft Robotics combining with Liquid Metal (LM)

3.1 Introduction

In this chapter, we present a novel method to actuate the robot with a more flexible and robust material which is liquid metal. Based on the study of liquid metal (Table 1-1), we combined LCE and LM together, and such LCE/LM system shows amazing robustness, consistency and repeatability in bending and shrinking performance. Besides, LCE strip was tried to be programmed in a deviated direction, in this case, the robot shows the ability to twist when external stimulus was applied.

Two methods combining liquid metal have been developed, for both fabricated system, the dynamic deformation performances were recorded.

The same as what we discussed in Chapter 1, the system's performance shows an enhancement when current input increases.

Based on this system, several bio-simulation of walking robot were designed and fabricated, accessories (needle tips, etc.) were integrated into the robot to provide mobility. Caterpillar climbing was also simulated by designed robot composed of three actuating parts.

3.2 Preparation of LCE/LM system

In this section, LCE segments and patterned liquid metal were integrated. The LCE was prepared using a two-stage thiol-acrylate Michael addition-photopolymerization (TAMAP) reaction. 4-bis-[4-(3-acryloyloxypropyl)oxy]benzoyloxy]-2-methylbenzene (RM257), pentaerythritol tetrakis(3-mercaptopropionate) (PETMP), 2,2-(ethylenedioxy)diethanethiol (EDDET), (2-hydroxyethoxy)-2-methylpropiophenone (HHMP) and dipropylamine (DPA) which were used as received purchasing from Sigma Aldrich except RM257 bought from Wilshire Technologies. 4g of RM257, 0.217g of PETMP, 0.9157g of EDDET and 0.0257g of HHMP were dissolved into 1.6g of toluene solution. 0.568g of DPA (diluted with toluene at a ratio of 1:50) was added into solution for the first polymerization then cured at 80°C for 12h. The cured polymer was then aligned by stretching and exposed to UV light for at least 15mins as the second polymerization. The liquid metal (99.99% purity of Gallium) bought from Phitoon was used as the stimulator. First, in the preparation of liquid metal channel mask, a layer of paper sheet and another layer of double-side tape was integrated together, then the composite was cut by laser cutter where the designed pattern was input before, after cutting out the channel part, the edge was cleaned in Acetone. Second, the fabricated mask was then taped onto VHB tape layer (3M VHB™) which was already fixed onto an acrylate plate, followed by Gallium (in liquid phase) casting onto the mask and flowing into the channel.

A glass slice was then pressed upon the channel to fix the final shape of liquid metal. Third, the whole system was then cooled down under room temperature, the glass slice could be then easily peeled off, so did the channel mask. Varieties of mask could be designed to achieve various functions. After the liquid metal was patterned and cooled down to solid phase, a piece of LCE segment was taped onto the liquid metal by VHB tape.

An optional method is to cast PDMS layer onto the LCE/LM system used as passive and encapsulate layer. PDMS was prepared by homogenously mixing silicone elastomer and curing agent (Sylgard 184, Dow Coming) in a weight proportion of 5:1. The thorough mixture was then degassed in a vacuum desiccator for 40mins to remove all trapped air bubbles. After degassing, the liquid mixture was cast onto LCE/LM system until curing.

3.3 LCE/LM System Deformation Performance

Several patterns of LCE/LM system have been fabricated. To present a basic demonstration of its deformation performance, a simple robot composed of two LCE/LM systems were integrated together with a layer of VHB tape. The performances were recorded as Figure 3-1 showing.

In the Figure 3-1(A), it depicts the cross section of this composite which combines of two LCE/LM bonded by a layer of VHB tape. For the LCE segment, the program direction determines monomer chain's alignment, as

well as sample's bending direction when external stimulus is applied. Two program directions have been proposed, one is right along center line of sample, while another one is along the diagonal. In this case, linear shrinking of about 45% maximum linear strain, two-way bending would be observed for former alignment, while twisting would be observed for latter one.

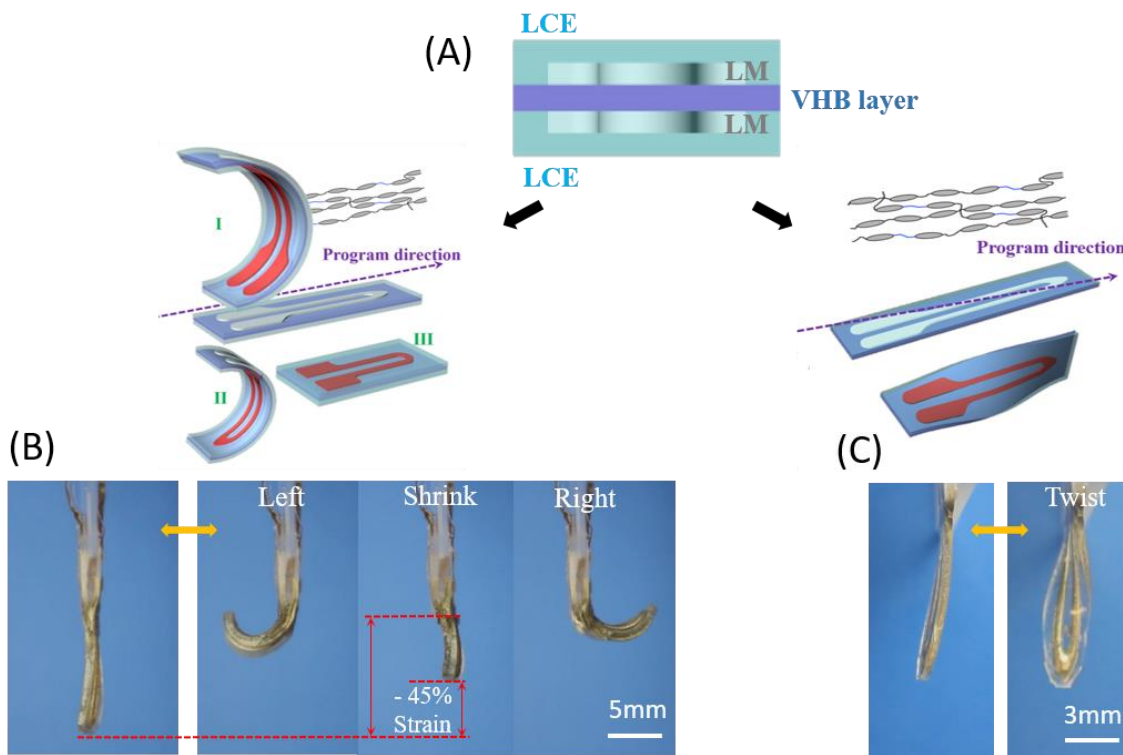


Figure 3-1. Configuration of LCE/LM system and its performance. (A) A basic demonstration of robot composed of two LCE/LM system, and their difference in program direction inducing different bending orientation. (B) Center line-programmed robot in original shape (left one); Bending left (left two); Linear shrinking of 45% strain (right two); Bending right (right one) (C) Diagonal-programmed robot in original shape (left); Twisting phase (right)

For the former robot which is center line-programmed, the performance is controlled by actuating corresponding system. When left system is stimulated, the whole robot bends towards left due to shortened length of left side; The same phenomenon could be observed for the right side; When both system is stimulated, the robot would perform a linear shrinking because of shortened length in both systems. For the latter one which is diagonal-programmed, the robot shows a twisting performance when both systems are stimulated. All of the deformation is reversible when the current is off.

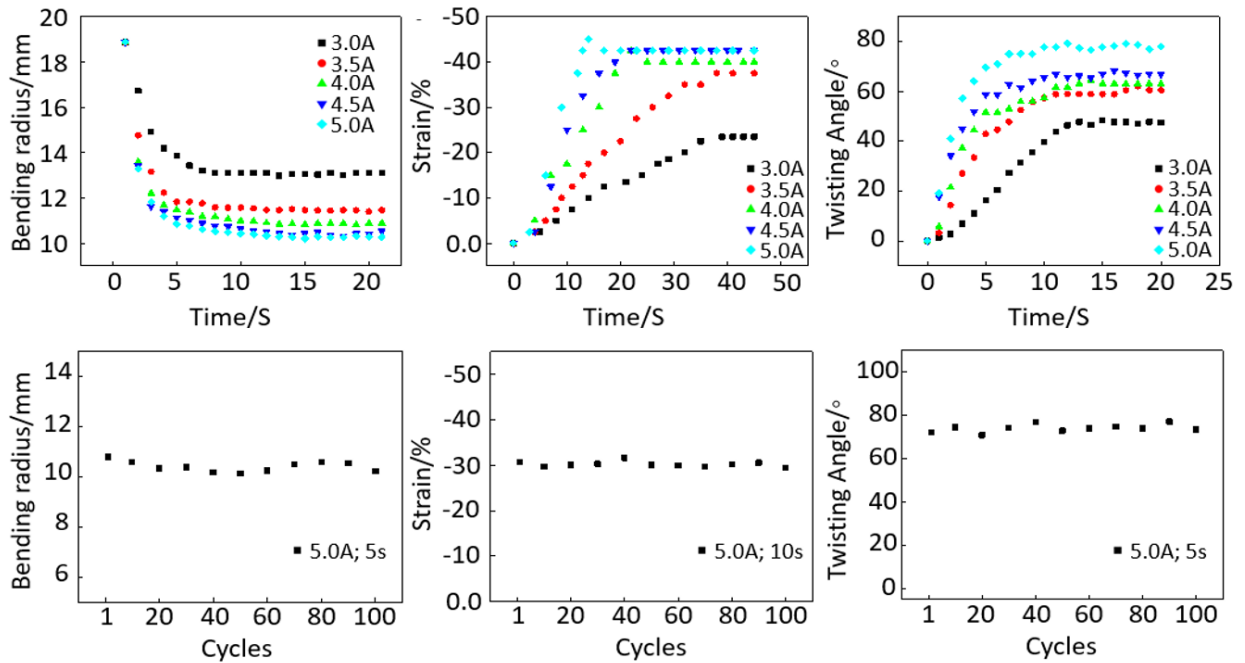


Figure 3-2. Dynamic bending radius (left top); shrinking strain (middle top) and twisting angle (right top). 100 cycles of bending (left bottom); shrinking strain (middle bottom) and twisting angle (right bottom)

Besides, to quantify the performance of this system, we also observed the phenomena and recorded the dynamic bending radius, strain and twisting

angle under different current input as shown in Figure 3-2. Varied of current input from 3A to 5A were applied to the robot. We can tell from the figures that with increasing of current input, the system bending amplitude, linear strain and twisting angle increase significantly then reach a plateau and stabilize. The comprehensive performance was enhanced with increment of current input and 5A is the optimal condition for its least bending radius of 10mm, largest shrinking strain of 45% and largest twisting angle of 80°. Also, repeatability test was conducted, the test was performed at 5A input and several seconds of interval to cool down the system. Over 100 cycles of bending, shrinking and twisting, the LCE/LM system shows its robustness and consistency of the performance. The bending radius maintains around 10mm, strain of 30% and twisting of 70°.

3.4 Fabrication of Enhanced Robot

To obtain an improvement of walking robot based on those integrated with solid flexible electronics, some novel designation of robot was brought out and fabricated. For these robots, the movement is not as simple as showing in basic demonstration which unique LCE segment is enough to achieve all the functions, the synergy of multiple LCE segments is required to accomplish a complex movement. However, the actuators could not be bonded well in one plane due to its terrible adhesion, hence, PDMS as a passive material is used

here to connect the segments together as an enhancement. Based on this consideration, we designed the composite as shown in Figure 3-3. The fabrication process is displayed in Figure 3-3 (A), first, the liquid metal is cast onto channel mask and solidify on the VHB layer surface, then, PDMS is cast on the liquid metal until curing in room temperature in case of damage on interface. At last, the sample is flipped over and taped with LCE segment. By casting second layer of PDMS, all the segments could be connected. The VHB tape between liquid metal and LCE shows great adhesion, also, PDMS works as passive and encapsulating layer could be bonded well.

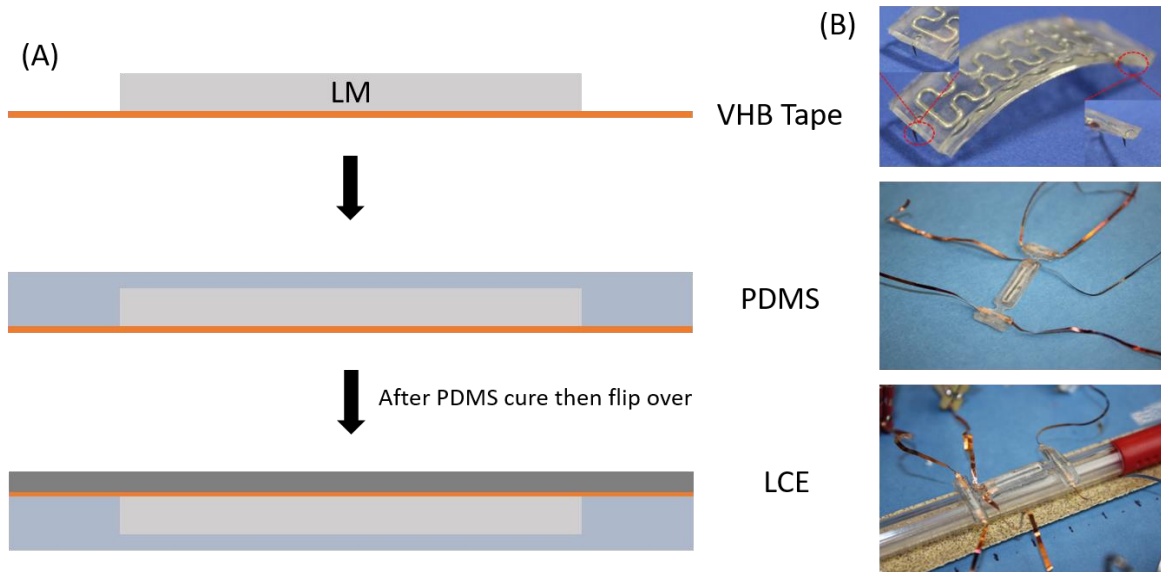


Figure 3-3. (A) Illustration of fabrication process, liquid metal is sandwiched by PDMS layer and LCE layer. (B) Needle tip equipped robot (top); Two types of caterpillar-simulated robot with different size of grasping feet.

Based on this LCE/LM system, soft robots in different shapes to achieve different functions have been fabricated. As shown in Figure 3-3 (B), for the top one, needle tip is integrated underneath the robot by a certain angle so it

could move forward only by bending and relaxing its body. The second and third robots are designed to simulate caterpillar which will grasp a stick then move. Three LCE segments are connected by passive PDMS layer, two actuators as grasping feet were designed on the head and tail parts, the other one as body part to bend. By arching and relaxing the body, these two robots could achieve moving forward and backward.

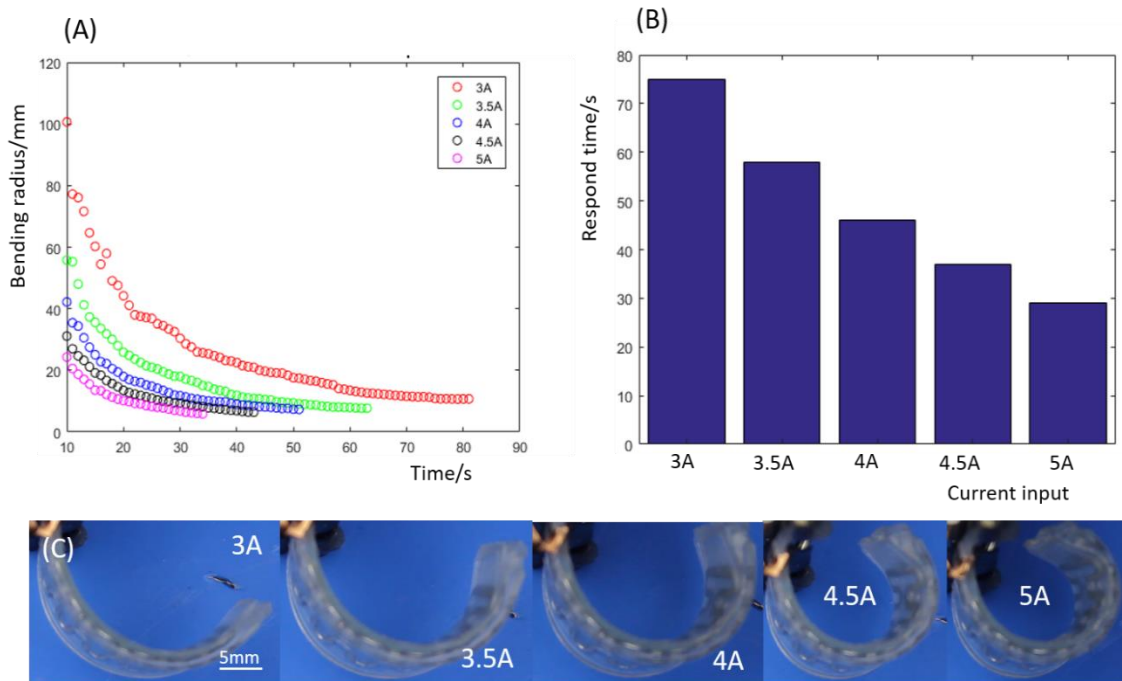


Figure 3-4. (A) Dynamic bending radius for the robot under varied current input. The bending radius continues go down with accumulation of generated heat. (B) Respond time of robot. (C) Visualization of robot's ultimate states under each current input. Under 5A input, the robot reaches and maintains at maximum bending curvature in the shortest respond time.

The basic bending test of robot shown in Figure 3-3 (B) top was conducted.

And the results are displayed in Figure 3-4. Figure 3-4 (A) records the dynamic bending radius under varied current input. Figure 3-4 (B) illustrates

the respond time. Figure 3-4 (C) visualizes the ultimate state for the robot under each current input. When 5A is applied, the largest deformation amplitude could be observed among all the circumstances, 5mm of bending radius is achieved under this condition and takes only 30 seconds to reach the maximum bending amplitude.

3.5 Conclusion

In this chapter, LCE/LM system is proposed for the improved performance in flexibility and consistency. In the demonstration of basic function part, the test upon bending, shrinking and twisting have been conducted, and results show their great deformation amplitude. The center line-programmed robot could reach at 10mm of bending radius and 45% of shrinking strain while the diagonal-programmed robot could achieve 80 degrees of twisting.

Besides, the repeatability test concludes that such LCE/LM system shows great consistency and robustness over 100 cycles, i.e., the fatigue life is elongated with introduction of liquid metal.

Based on this system, several prototypes of walking robots have been designed and fabricated, later test and improvement will be brought out for them.

Chapter 4. Reversibly Deformable Robotics blend into Surroundings

4.1 Introduction

In this chapter, camouflage phenomena in nature is studied. As one of the most intriguing research field, camouflage is the method for animal concealment that blend themselves into surroundings to avoid detection of predators and prey for surviving. Chameleon is the most straightforward example that they could easily vanish in bush by autonomously controlling surface color. Scientists have explored a lot in this field [31, 33-35].

The camouflage could be sorted as change in surface coloration, patterns, morphological skin and others (odor, noise, motion, etc.), in addition to the combination of changes above.

In this study, based on LCE/LM system, three primary deformable robotics are fabricated and showing great potential to hide themselves in environments. Three robotics simulate origami pentagon, sea plants and black agaric separately and the deformation is reversible when current is not applied. Besides, the introduction of tunable pigment provides the possibility to change surface color. At last, walking robot could be combined with camouflage system to grant the mobility to it.

4.2 Experimental Section

4.2.1 Preparation of Camouflage Robot

In this section, LCE segments and patterned liquid metal were integrated. The LCE was prepared using a two-stage thiol-acrylate Michael addition-photopolymerization (TAMAP) reaction. 4-bis-[4-(3-acryloyloxypropyl)oxy]benzoyloxy]-2-methylbenzene (RM257), pentaerythritol tetrakis(3-mercaptopropionate) (PETMP), 2,2-(ethylenedioxy)diethanethiol (EDDET), (2-hydroxyethoxy)-2-methylpropiophenone (HHMP) and dipropylamine (DPA) which were used as received purchasing from Sigma Aldrich expect RM257 bought from Wilshire Technologies. 4g of RM257, 0.217g of PETMP, 0.9157g of EDDET and 0.0257g of HHMP were dissolved into 1.6g of toluene solution. 0.568g of DPA (diluted with toluene at a ratio of 1:50) was added into solution for the first polymerization then cured at 80°C for 12h. The cured polymer was then aligned by stretching and exposed to UV light for at least 15mins as the second polymerization. The liquid metal (99.99% purity of Gallium) bought from Phitoon was used as the stimulator. First, in the preparation of liquid metal channel mask, a layer of paper sheet and another layer of double-side tape was integrated together, then the composite was cut by laser cutter where the designed pattern was input before, after cutting out the channel part, the edge was cleaned in

Acetone. Second, the fabricated mask was then taped onto VHB tape layer (3M VHB™) which was already fixed onto an acrylate plate, followed by Gallium (in liquid phase) casting onto the mask and flowing into the channel. A glass slice was then pressed upon the channel to fix the final shape of liquid metal. Third, the whole system was then cooled down under room temperature, the glass slice could be then easily peeled off, so did the channel mask. Varieties of masks could be designed to simulate various stuffs. In this study, Eco-flex is used as the passive layer instead of PDMS for its quick curing and lower modulus. Eco-flex was prepared by homogenously mixing portions of 1A and 1B (Smooth-on, Inc, Eco-flex™) in a weight proportion of 1:1. The thorough mixture was then degassed in a vacuum desiccator for 5mins to remove all trapped air bubbles. After degassing, the liquid mixture was cast onto liquid metal channel until curing. On the back side of this system, LCE segments are taped onto the VHB layer, frictional powder is sprinkled on other exposed area to prevent VHB adhesion on ground.

4.2.2 Camouflage Phenomena Simulation

Three primary robots have been designed and fabricated as shown in Figure 4-1. Figure 4-1 (A) illustrates several patterns of soft robot, in the dashed line circles, LCE segments are embedded into Eco-flex, and connected by patterned liquid metal channel. The liquid metal is used to generate heat and

stimulate LCE segments which actuate deformation. Different shapes of robots have been fabricated to achieve specific functions. Figure 4-1 (B) and Figure 4-1 (C) depicts the rest and actuation states of the camouflage

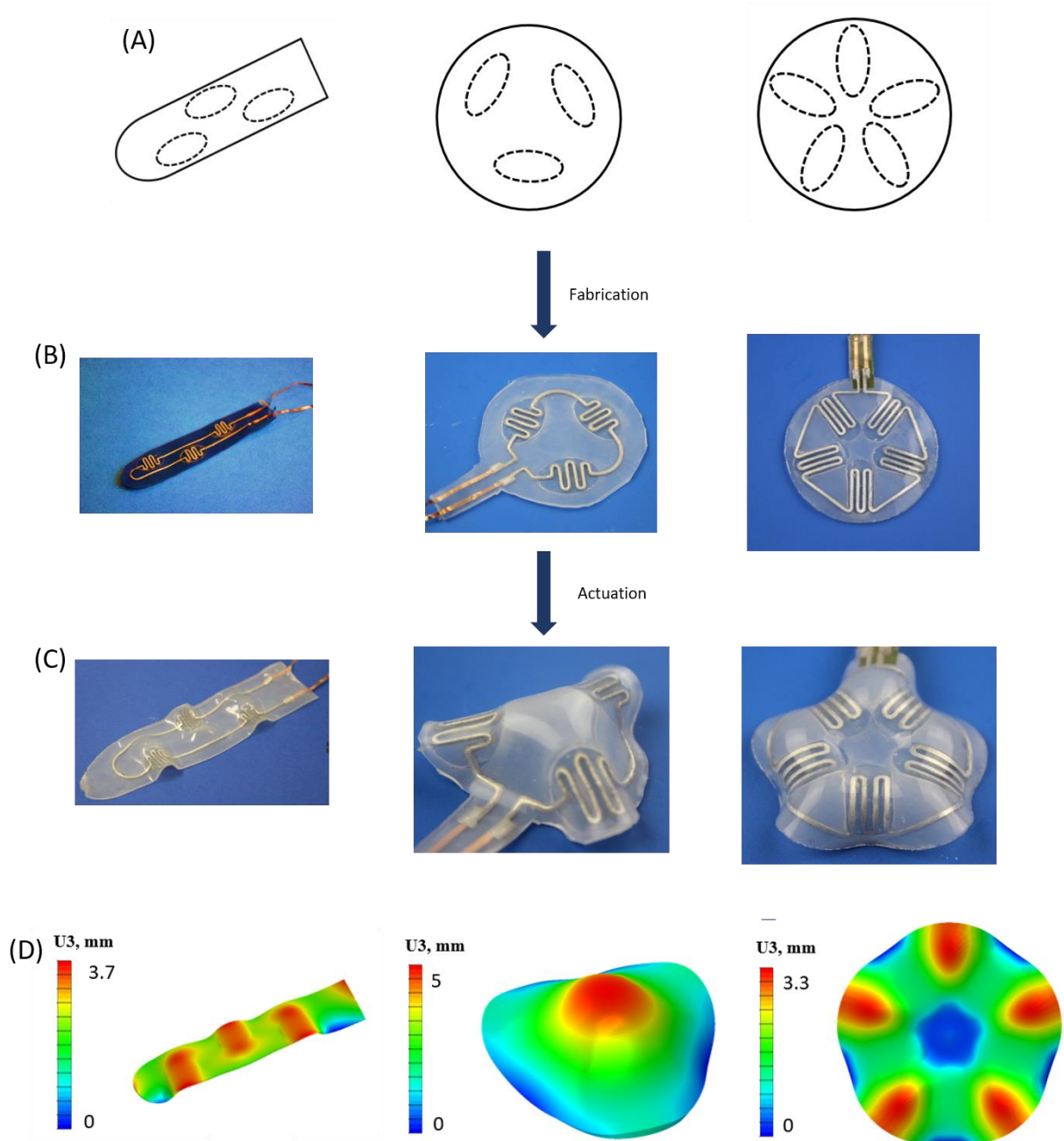


Figure 4-1. (A) Patterns of designed robot, solid circle indicates the area of passive Eco-flex, and dashed circle for LCE segments. (B) Visualization of robots in rest

state. (C) Visualization of robots in actuation state. (D) FEA analysis for each robot system, displacements in U3 direction are displayed.

robot. Figure 4-1 (D) shows the FEA analysis showing approximate displacement in U3 direction indicating the deformation amplitude. The first robot could achieve 3.7mm displacement in vertical direction, while 5mm for the second one and 3.3mm for the third one.

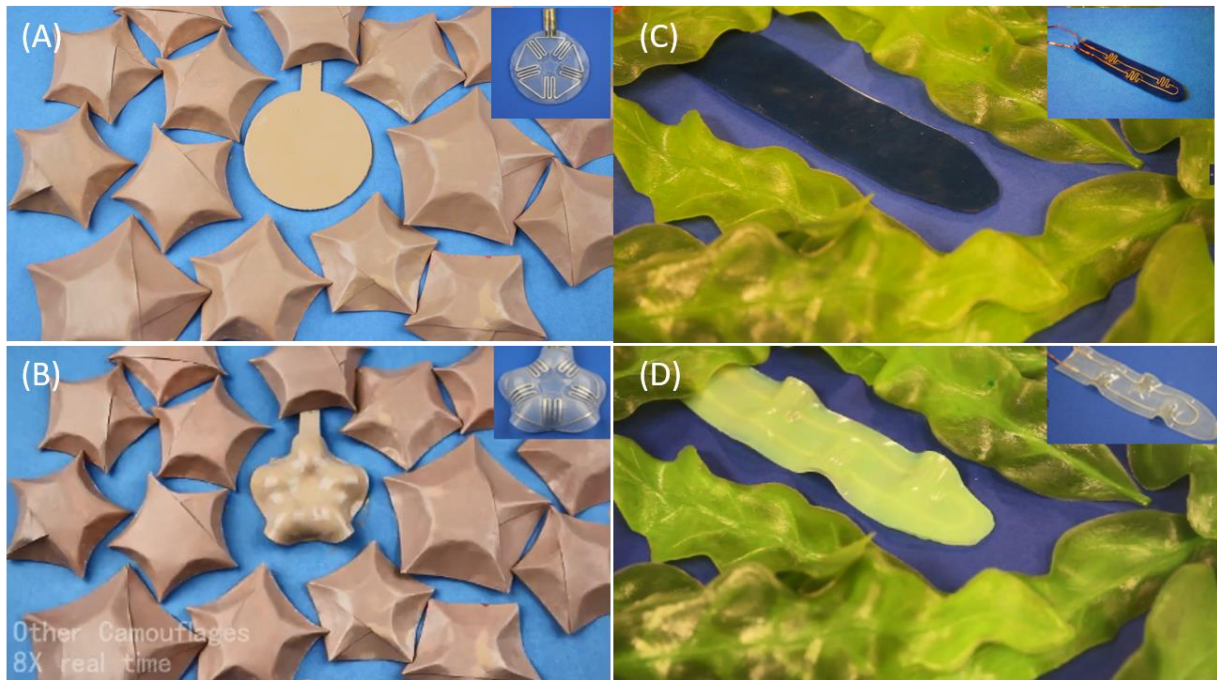


Figure 4-2. Deformation of camouflage robots (A) Five LCE segments-integrated robots in rest state. (B) Actuation state of the robot simulating an origami pentagon. (C) Three LCE segments-robot in rest state. (D) The actuated robot simulating a seaweed by change in both color and shape.

For the next step, two of the designed soft robots are placed in two man-made environments respectively. Figure 4-2 shows the rest state and ultimate state of these two robots. In Figure 4-2 (A), the robot is painted with similar color as surrounded origami pentagons. When it is actuated, the camouflage robot

changes its shape to simulate the surroundings (Figure 4-2 (B)). In Figure 4-2 (C), the robot colored with tunable pigment that controlled by temperature is placed around with seaweed. When it is actuated, the robot changes not only the shape from flat to wrinkled but also the color from black to green (Figure 4-2 (D)). Figures here display the significant diversity between normal and actuation states. The insets of figures depict their original colors without painting, and liquid metal channels are visible. These two examples show their great potential to disguise themselves by actuating with current based on this easy-manufacturable LCE/LM system.

Apart from camouflage in stationary, a moving-camouflaging robot has also been designed that combines crawling robot equipped with needle tips as we discussed before and camouflage system painted black. The whole system is bonded just by some droplets of PDMS. At first, the crawling robot carrying camouflage system walks to black agaric from a long distance away. Then when it's surrounded by the fungi, camouflage robot is actuated and deform itself to simulate the surroundings. Figure 4-3 displays the synergy of crawling robot and camouflage system. What's more, by applying different amplitude of current, the deformation would vary and approach all kinds of fungi shape. The Figure 4-3 (A) shows the mobility of such system, the robot could walk in a specific direction from long distance away. Figure 4-3 (B) displays the reversible camouflage ability. Figure 4-3 (C) illustrates the idea

of crawling robot that integrated with needle tips underneath the body at a specific angle providing movement friction. Figure 4-3 (D) depicts the visualization of this whole system, some PDMS droplets (blue spot) is employed to bond the camouflage system (top) and crawling robot (bottom).

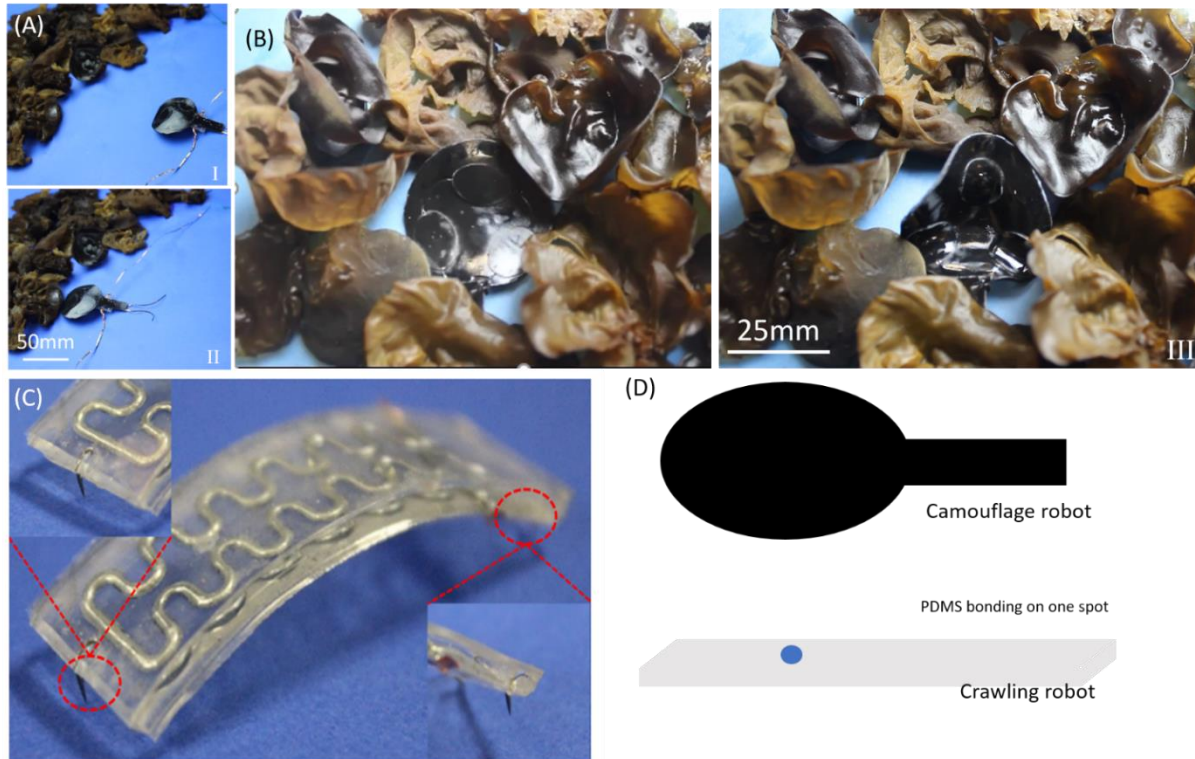


Figure 4-3. Illustration of moving-camouflaging robot (A) Crawling robot carrying the camouflage system walks to black agaric from a long distance away. (B) Camouflage system blend into surroundings by actuating three LCE segments. (C) Configuration of crawling robot. (D) Methods to bond the camouflage system and crawling robot together.

4.3 Conclusion

In this chapter, a robust, simple way to deform designed robots reversibly is developed using LCE/LM system for its impressive large deformation and robustness. To be specific, shape changing achieved by LCE segments and

color changing accomplished by tunable pigments are employed to disguise the camouflage system as origami pentagons, sea plants and black agaric. The introduction of crawling robot grants legless camouflage system mobility to move towards specific orientation. In the future work, 3d printing of LCE/LM system will be preferred to improve its compatibility and adaptability in extreme harsh environment. We will also study and simulate more complex surface like chameleon and cephalopod skin deformation based on the foundation of LCE/LM system.

Chapter 5. Summary and Prospects

5.1 Summary

In this dissertation, applications of liquid crystalline elastomers (LCEs) have been explored with the introduction of solid flexible electronics (aluminum foil) and liquid metal (Gallium). Several soft robots have been developed simply and economically for a wide range of bio-simulation as inchworm movement, caterpillar grasping and moving, and camouflage phenomena in nature. The fabrication approaches and experimental setups in this dissertation find the possibility to realize accessible actuation for large controllable deformation of soft robots. The dissertation also sets down a profound significance in robust soft robots and inspiration of camouflage system.

First, in chapter 2, the performance of LCE samples in different thickness under varied current input have been presented some conclusions are taken out that the maximum bending curvature is proportional to current input, Thickened robot impedes its movement in both responding time and maximum bending amplitude. Besides, two types of inchworm robot have been proposed, accessories such as sandpaper and 3d printed legs are equipped to move the robots, based on which, more methods to increase mobility will be inspired for the future. Then, in chapter 3, the development of LCE/LM system grants the soft robot extreme high robustness and

significantly improved flexibility. Gallium in liquid phase owns larger thermal and electrical conductivity which allows it to generate and conduct heat through the robot freely. Also, continuity of such heat stimulator is not worth considered for its liquid properties. At last, in chapter 4, camouflage phenomena in nature is studied, and based on reviewing of progression in this research field, several robots that could simulate surroundings have been proposed. Two most interesting points are introduction of tunable pigments and combination with crawling robots. Both methods show enhancements for legless camouflage robot that deforms only.

5.2 Prospects

LCE as a smart material shows great potential in soft robotics field for its significant reversible deformation upon external stimuli. The respond speed may not as fast as dielectric, hydraulic or pneumatic materials that rely on embedded actuators, however, the change in molecular chain structure expects the robot fabricated in micro even nanoscale which is impossible for those non-molecular level actuations.

For future work, these goals will be on the top considerations: the first is to reduce wiring constraints which could affect absolute movement of robot.

Alternative solutions could be like using a thinner and longer copper wire to conduct and different heater designs; the second is to develop 3d printing of

LCE or LCE/LM system to fabricate desired shape of soft robot, in this case, more complex robot that complete diverse missions especially in harsh environments will be compatible; the third is to employ the robot in varieties of jobs, such as grasping and holding grapes, eggs and even larger stuffs. In addition, if the microscopic fabrication is developed, drug delivery or organic surgery like cardiac transplant could be accomplished; the fourth goal is to develop its self-sensing reacting and bending/pressure detection, which provides the possibility for robot used in biological embedment to sense and collect signals from inside the human body. At last, to simulate more complicated camouflage phenomena in nature, the mechanism of morphological surface will be studied and discussed, accessible approaches will be brought up.

Bibliography

- [1] J. Rossiter, P. Walters & B. Stoimenov, "Printing 3D dielectric elastomer actuators for soft robotics," Proc. SPIE 7287, Electroactive Polymer Actuators and Devices (EAPAD) 2009, 72870H (6 April 2009).
- [2] S. Shian, K. Bertoldi & D. R. Clarke. Dielectric Elastomer Based "Grippers" for Soft Robotics. *Adv. Mater.* 2015, 27, 6814–6819.
- [3] J. Shintake, B. Schubert, S. Rosset, H. Shea & D. Floreano, Variable Stiffness Actuator for Soft Robotics Using Dielectric Elastomer and Low-Melting-Point Alloy. *2015 IEEE/RSJ International Conference on Intelligent Robots and Systems (IROS)*, 1097-1102
- [4] S. Kim, E. Hawkes, K. Choy, M. Joldaz, J. Foley & R. Wood. Micro artificial muscle fiber using NiTi spring for soft robotics. *2009 IEEE/RSJ International Conference on Intelligent Robots and Systems*, 2228-2234.
- [5] S. Seok, C. D. Onal, R. Wood, D. Rus & S. Kim. Peristaltic locomotion with antagonistic actuators in soft robotics, *2010 IEEE International Conference on Robotics and Automation, Anchorage Convention District*, 1228-1233.
- [6] R. F. Shepherd, A. A. Stokes, J. Freake, J. Barber, P. W. Snyder, A. D. Mazzeo, L. Cademartiri, S. A. Morin & G. M. Whitesides, Using Explosions to Power a Soft Robot, *Angew. Chem.* 2013, 125, 2964 –2968.
- [7] S. Yim & M. Sitti, Shape-Programmable Soft Capsule Robots for Semi-Implantable Drug Delivery, *IEEE TRANSACTIONS ON ROBOTICS*, VOL. 28, NO. 5, OCTOBER 2012, 1198-1202.
- [8] S. Yim & M. Sitti, Design and Rolling Locomotion of a Magnetically Actuated Soft Capsule Endoscope, *IEEE TRANSACTIONS ON ROBOTICS*, VOL. 28, NO. 1, FEBRUARY 2012, 183-194.
- [9] R. Fuhrer, E. K. Athanassiou, N. A. Luechinger & W. J. Stark, Crosslinking Metal Nanoparticles into the Polymer Backbone of Hydrogels Enables Preparation of Soft, Magnetic Field-Driven Actuators with Muscle-Like Flexibility, *small*, 2009, 5, No. 3, 383–388.
- [10] H. Zeng, P. Wasylczyk, C. Parmeggiani, D. Martella, M. Burreli, & D. Sybolt Wiersma, Light-Fueled Microscopic Walkers, *Adv. Mater.* 2015, 27, 3883–3887.
- [11] C. Li, Y. Liu, X. Huang & H. Jiang, Direct Sun-Driven Artificial Heliotropism for Solar Energy Harvesting Based on a Photo-Thermomechanical Liquid-Crystal Elastomer Nanocomposite, *Adv. Funct. Mater.* 2012, 22, 5166–5174.

- [12] A. Lendlein, H. Jiang, O. Junger & R. Langer, Light-induced shape-memory polymers, *Nature*, VOL 434, 14 April 2005, 879-882.
- [13] J. Mohd Jani, M. Leary, A. Subic & M. A. Gibson, A review of shape memory alloy research, applications and opportunities, *Materials and Design*, 56 (2014) 1078–1113.
- [14] C. Chluba, W. Ge, R. L. de Miranda, J. Strobel, L. Kienle, E. Quandt & M. Wuttig, Ultralow-fatigue shape memory alloy films, *Science*, 29 May 2015, VOL 348, ISSUE 6238, 1004-1008.
- [15] Q. Zhao, H. J. Qi, T. Xie, Recent progress in shape memory polymer: New behavior, enabling materials, and mechanistic understanding, *Progress in Polymer Science*, 49–50 (2015) 79–120.
- [16] A. Sánchez-Ferrer, T. F., M. Stubenrauch, A. Albrecht, H. Wurmus, M. Hoffmann & H. Finkelmann, Liquid-Crystalline Elastomer Microvalve for Microfluidics, *Adv. Mater.* 2011, 23, 4526–4530.
- [17] W. Hu, H. Cao, Li Song, H. Zhao, Si. Li, Z. Yang & H. Yang, Thermally Controllable Reflective Characteristics from Rupture and Self-Assembly of Hydrogen Bonds in Cholesteric Liquid Crystals, *The Journal of Physical Chemistry Letters*, 2009, 113, 13882-13885
- [18] T. H. Ware, M. E. McConney, J. J. Wie, V. P. Tondiglia, T. J. White, Voxellated liquid crystal elastomers, *Science*, 27 February 2015, VOL 347 ISSUE 6225, 982-985.
- [19] A. Buguin, M-H. Li, P. Silberzan, B. Ladoux & P. Keller, Micro-Actuators When Artificial Muscles Made of Nematic Liquid Crystal Elastomers Meet Soft Lithography, *J. AM. CHEM. SOC.* 2006, 128, 1088-1089
- [20] M. Camacho-Lopez, H. Finkelmann, P. Palffy-Muhoray & M. Shelley, Fast liquid-crystal elastomer swims into the dark, *nature materials*, VOL 3 MAY 2004, 307-310.
- [21] Michael T. Tolley, Robert F. Shepherd, Bobak M., Kevin C. Galloway, M. Wehner, M. Karpelson, Robert J. Wood & George M. Whitesides, A Resilient, Untethered Soft Robot, *SOFT ROBOTICS*, Volume 1, Number 3, 2014, 213-223.
- [22] N. W. Bartlett, Michael T. Tolley, Johannes T. B. Overvelde, James C. Weaver, B. Mosadegh, K. Bertoldi, G. M. Whitesides, Robert J. Wood, A 3D-printed, functionally graded soft robot powered by combustion, *Science*, 10 July 2015, VOL 349 ISSUE 6244, 161-166.
- [23] E. Acome, S. K. Mitchell, T. G. Morrissey, M. B. Emmett, C. Benjamin, M. King, M. Radakovitz, C. Keplinger, Hydraulically amplified self-healing electrostatic actuators with muscle-like performance, *Science*, 359, 61–65 (2018).

- [24] M. Duduta, David R. Clarke, Robert J. Wood, A High Speed Soft Robot Based on Dielectric Elastomer Actuators, *2017 IEEE International Conference on Robotics and Automation (ICRA)*, 4346-4351.
- [25] R. K. Katzschmann, Andrew D. Marchese & D. Rus, Hydraulic Autonomous Soft Robotic Fish for 3D Swimming, *Experimental Robotics: The 14th International Symposium on Experimental Robotics*, June 2014, (pp.405-420).
- [26] C. Ohm, M. Brehmer & R. Zentel, Liquid Crystal Elastomers: Materials and Applications, 3 March 2012, 50-54.
- [27] Wei Wang, Jang-Yeob Lee, Hugo R., Sung-Hyuk Song, Won-Shik Chu & Sung-Hoon Ahn, Locomotion of inchworm-inspired robot made of smart soft composite (SSC), *Bioinspir. Biomim.* 9 (2014) 046006.
- [28] S. M. Felton, Michael T. Tolley, Cagdas D. Onal, Daniela Rus, and Robert J. Wood, Robot Self-Assembly by Folding a Printed Inchworm Robot, *2013 IEEE International Conference on Robotics and Automation (ICRA)*, 277-282.
- [29] H. Guo, J. Zhang, Tao Wang, Y. Li, Jun Hong, Yue Li, Design and Control of an Inchworm-Inspired Soft Robot with Omega-Arching Locomotion, *2017 IEEE International Conference on Robotics and Automation (ICRA)*, 4154-4159.
- [30] N. Lobontiu, M. Goldfarb, E. Garcia, A piezoelectric-driven inchworm locomotion device, *Mechanism and Machine Theory*, Volume 36, Issue 4, 1 April 2001, 425-443.
- [31] S. A. Morin, R. F. Shepherd, Sen Wai Kwok, Adam A. Stokes, Alex N., G. M. Whitesides, Camouflage and Display for soft machines, *Science*, 17 August 2012, VOL 337, 828-833.
- [32] S. Bauer, S. Bauer-Gogonea, I. Graz, Martin K., C. Keplinger & R. Schwödiauer, 25th Anniversary Article: A Soft Future: From Robots and Sensor Skin to Energy Harvesters, *Adv. Mater.* 2014, 26, 149–162.
- [33] Md. A. Haque, T. Kurokawa, Gen Kamita, Y. Yue & J. P. Gong, Rapid and Reversible Tuning of Structural Color of a Hydrogel over the Entire Visible Spectrum by Mechanical Stimulation, *Chem. Mater.* 2011, 23, 5200–5207.
- [34] Q. Zhao, A. Haines, D. Snoswell, C. Keplinger, R. Kaltseis, S. Bauer, I. Graz, R. Denk, Peter Spahn, G. Hellmann & J. J. Baumberg, Electric-field-tuned color in photonic crystal elastomers, *APPLIED PHYSICS LETTERS*, 100, 101902 (2012),
- [35] D. van den Ende, Jan-Dirk Kamminga, A. Boersma, T. Andritsch & Peter G. S., Voltage-Controlled Surface Wrinkling of Elastomeric Coatings, *Adv. Mater.* 2013, 25, 3438–3442.

- [36] Collin B. Eaker & Michael D. Dickey, Liquid metal actuation by electrical control of interfacial tension, *Applied Physics Reviews* 3, 031103 (2016).
- [37] D. J. Lipomi, M. Vosgueritchian, Benjamin C-K. Tee, S. L. Hellstrom, J. A. Lee, C. H. Fox & Z. Bao, Skin-like pressure and strain sensors based on transparent elastic films of carbon nanotubes, *Nature Nanotechnology*, VOL 6 DECEMBER 2011, 788-792.
- [38] Y-L. Park, B-R. Chen & Robert J. Wood, Design and fabrication of soft artificial skin using embedded microchannels and liquid conductors, *IEEE SENSORS JOURNAL*, VOL. 12, NO. 8, AUGUST 2012, 2711-2718.
- [39] H-J. Kim, C. Son & B. Ziaie, A multiaxial stretchable interconnect using liquid-alloy-filled elastomeric microchannels, *APPLIED PHYSICS LETTERS* 92, 011904 (2008).
- [40] J. Park, S. Wang, M. Li, C. Ahn, J. K. Hyun, D. S. Kim, Do K. Kim 1, J. A. Rogers, Y. Huang & S. Jeon, Three-dimensional nano networks for giant stretchability in dielectrics and conductors, *NATURE COMMUNICATIONS*, 2012, 3:916, DOI: 10.1038.
- [41] S. Zhu, J-H. So, Robin Mays, S. Desai, W. R. Barnes, B. Pourdeyhimi & Michael D. Dickey, Ultrastretchable Fibers with Metallic Conductivity Using a Liquid Metal Alloy Core, *Adv. Funct. Mater.* 2013, 23, 2308–2314.
- [42] John W. Boley, Edward L. White & Rebecca K. Kramer, Mechanically Sintered Gallium–Indium Nanoparticles, *Adv. Mater.* 2015, 27, 2355–2360.
- [43] J-H. Soa & Michael D. Dickey, Inherently aligned microfluidic electrodes composed of liquid metal, *Lab Chip*, 2011,11, 905-911.
- [44] N. Pekas, Q. Zhang & David Juncker, Electrostatic actuator with liquid metal–elastomer compliant electrodes used for on-chip microvalving, *J. Micromech. Microeng.* 22 (2012) 097001.
- [45] Y. Liu, M. Gao, S. Mei, Y. Han & J. Liu, Ultra-compliant liquid metal electrodes with in-plane self-healing capability for dielectric elastomer actuators, *Appl. Phys. Lett.* 103, 064101 (2013).
- [46] K-Q. Ma, J. Liu, Nano liquid-metal fluid as ultimate coolant, *Physics Letters A* 361 (2007) 252–256.
- [47] J. Y. Zhu, S-Y. Tang, K. Khoshmanesh & K. Ghorbani, An integrated Liquid Cooling System Based on Galinstan Liquid Metal Droplets, *ACS Appl. Mater. Interfaces*, 2016, 8, 2173–2180.
- [48] J-H. So, J. Thelen, A. Qusba, G. J. Hayes, G. Lazzi & Michael D. Dickey, Reversibly deformable and mechanically tunable fluidic antennas, *Adv. Funct. Mater.* 2009, 19, 3632–3637.

- [49] S. Cheng, Z. Wu, P. Hallbjörner, K. Hjort & A. Rydberg, Foldable and stretchable liquid metal planar inverted cone antenna, *IEEE Transactions on Antennas and Propagation*, VOL. 57, NO. 12, DECEMBER 2009, 3765-3771.
- [50] Z. Wu, K. Hjort & S. H. Jeong, Microfluidic stretchable RF electronics, *Proceedings of the IEEE*, Vol. 103, No. 7, July 2015, 1211-1225.
- [51] M. Kubo, X. Li, C. Kim, M. Hashimoto, B. J. Wiley, D. Ham & G. M. Whitesides, Stretchable microfluidic radiofrequency antennas, *Adv. Mater.* 2010, 22, 2749–2752.
- [52] G. J. Hayes, J-H. So, A. Qusba, Michael D. Dickey & G. Lazzi, Flexible liquid metal alloy (EGaIn) microstrip patch antenna, *IEEE Transactions on Antennas and Propagation*, VOL. 60, NO. 5, MAY 2012, 2151-2156.
- [53] A. T. Ohta, S. Guo, B. J. Lei, W. Hu & W. A. Shiroma, A liquid-metal tunable electromagnetic-bandgap microstrip filter, *Wireless Information Technology and Systems (ICWITS), 2012 IEEE International Conference*.
- [54] A. J. King, J. F. Patrick, N. R. Sottos, S. R. White, G. H. Huff & J. T. Bernhard, Microfluidically switched frequency-reconfigurable slot antennas, *IEEE ANTENNAS AND WIRELESS PROPAGATION LETTERS*, VOL. 12, 2013, 828-831.
- [55] C. Koo, B. E. LeBlanc, M. Kelley, H. E. Fitzgerald, G. H. Huff & Arum Han, Manipulating Liquid Metal Droplets in Microfluidic Channels with Minimized Skin Residues Toward Tunable RF Applications, *Journal of Microelectromechanical Systems*, VOL. 24, NO. 4, AUGUST 2015, 1069-1076.
- [56] S. H. Jeong, A. Hagman, K. Hjort, M. Jobs, J. Sundqvist & Z. Wu, Liquid alloy printing of microfluidic stretchable electronics, *Lab Chip*, 2012, 12, 4657–4664.
- [57] J-S. Koh, K-J. Cho, Omegabot: biomimetic inchworm robot using SMA coil actuator and smart composite microstructures (SCM), *Proceedings of the 2009 IEEE International Conference on Robotics and Biomimetics*, 1154-1159.
- [58] D. Lee, S. Kim, Y-L. Park & Robert J. Wood, Design of centimeter-scale inchworm robots with bidirectional claws, *2011 IEEE International Conference on Robotics and Automation (ICRA)*, 3197-3204.
- [59] S. Ueno, K. Takemura, S. Yokota & K. Edamura, An inchworm robot using electro-conjugate fluid, *Proceedings of the 2012 IEEE, International Conference on Robotics and Biomimetics*, 1017-1022.